3-D GAMMA KNIFE DOSE DISTRIBUTION BY NORMOXIC GEL DOSIMETRY NEAR TISSUE INHOMOGENETIES

by

Fatih Isbakan

BSc. Physics, Bogaziçi University, 1993
MSc. Biomedical Engineering, Bogaziçi University, 1997

Submitted to the Institute of Biomedical Engineering
in partial fulfillment of the requirements
for the degree of
Doctorate of Philosophy
In
Biomedical Engineering

Bogaziçi University
2005

3-D GAMMA KNIFE DOSE DISTRIBUTION BY NORMOXIC GEL DOSIMETRY NEAR TISSUE INHOMOGENETIES

APPROVED BY:

Prof. Yekta ULGEN ..…….

(Thesis Supervisor)

Prof Yani SKARLATOS .....…….....

Assoc Prof Hatice BILGE ….....

Assoc Prof Meriç SENGÖZ ……..

Assoc Prof Albert GÜVENIS ……..……

DATE OF APPROVAL:

ACKNOWLEDGMENTS

To my beloved daughter Ece Beyza Isbakan,

Many wonderful people have helped me to go in right direction the progress and completion of this thesis. I would like to express my gratitude to all of them.

I am deeply indebted to my advisor Prof. Yekta Ulgen for his time of research, writing of this thesis, helping, leading and encouraging me. His continuous support has helped me in overcoming the difficulties which came up during my doctoral program. Without him, this dissertation would not have been possible. I also thank Assoc. Prof. Hatice Bilge who always provided constructive and valuable comments during my thesis time. She has enlightened me on my way in difficult paths as well. I would like to thank Prof. Yani Skarlatos for his advises and inspiring discussions which obviously clarified my ideas.

Many special thanks go to my colleagues Bora Buyuksarac and Onur Agus from the Department of Biomedical Engineering Institute of Bogazici University. I want to thank them for all their great help, support, interest and valuable hints in the coding and analysis of the problems in this study.

I would like to give my special thanks to Zeynep Ozen who has helped me a lot in all the phases of this research. She was for sure the main contributor in this thesis.

Specials thanks to Öznur Özkesen for her great support in all our experiments.

I would also like to thank a lot to Inci Kartal for her great understanding and support during this long period of study. Without her tolerance and encouragement this thesis would not end.

My parents and my Sisters deserve special acknowledgement for their love and support through all these years.

Gary Berlind and Kay Oosthuisen looked closely at the final version of the thesis for English style and grammar, correcting both and offering suggestions for improvement.

The gels were prepared in the Chemistry department of Bogazici University laboratories. I present my thanks to Prof Selim Küsefoglu and Tarik Eren, PhD for their contributions.

ABSTRACT

3-D GAMMA KNIFE DOSE DISTRIBUTION BY NORMOXIC GEL DOSIMETRY NEAR TISSUE INHOMOGENETIES

The primary goal in this study was to investigate the three dimensional dose distributions, near the areas of tissue inhomogeneities, in Gamma Knife Radiosurgery with the normoxic gel dosimetry. Following irradiation, when scanned in MR and post processing the MR images, dose imparted to any particular point in the gel phantom can be calculated via the true T_2 relaxation time at that point. In the neighborhood of air-tissue inhomogeneity in the head, electronic disequilibrium can lead to errors in dose calculated with the treatment planning algorithms that presume the head as a homogeneous media. Two experiments were designed to investigate the inhomogeneity effects in the Gamma Knife radiosurgery: one experiment simulating the volume near the auditory canal cavity and, the other simulating the volume near the paranosal sinuses cavity. In the auditory canal cavity experiment, an identical balloon of a diameter of 16 cm with two corks placed on each side to represent the air cavities constitutes the inhomogeneous phantom. In the paranosal sinuses cavity experiment, a cylindrical cork is placed to represent the maximal sinuses. In both experiments, the homogeneous phantom is a spherical glass balloon filled with normoxic polymer gel. For dose calibrations, 100 ml vials filled with the same gel are irradiated at predefined doses, and the R_2-dose calibration curve is extracted. Dose distributions are the results of a single shot, by using all 201 Cobalt sources, delivered to a known point in the phantoms. In the aspect of dosimetrical quality control, the Gamma Knife planning system predicted dose distribution is compared with the experimental results. In the homogeneous phantoms, the gel dosimetry calculated dose distribution is in good agreement with the GammaPlan predicted dose distribution. However, in the case of inhomogeneous phantoms, the dose distribution is spatially different and significant differences in dose levels are observed. The dose decrease near the air-tissue interface causes the overshooting of the dose by the GammaPlan. This underdosing effect can be essential for the lesions near tissue inhomogeneities. In the auditory canal cavity experiment, the diameter of the 50% isodose curves differ by 35% in the X axis and 1% in the Y axis for Z=105 mm axial plane; and by 39% in the X axis and 5% in the Z axis for Y=105 mm coronal plane in the inhomogeneous phantom as compared to the homogeneous phantom. In the paranosal sinuses cavity experiment, the diameter of the 50% isodose curves differ by 42% in the X axis and 47 %in the Y axis for Z=71mm axial plane; 42% in the X axis and 60%in the Y axis for Z=75 mm axial plane; 52% in the X axis and 70% in the Y axis for Z=79 mm axial plane respectively in the inhomogeneous phantom when compared to the homogeneous phantom. The dose decrease near the air-tissue interface causes the Gamma Plan's predicted dosage to be higher than that actually delivered. The resulting underdosing effect can be critical for the control of the lesions near tissue inhomogeneities.

Keywords : Polymer Gel, Gel Dosimetry, Dose distribution, Tissue Inhomogeneity, Stereotactic Radiosurgery, Gamma Knife.

ÖZET

DOKU INHOMOJENITE YAKINLARINDA ÜÇ BOYUTLU GAMMA KNIFE DOZ DAGILIMININ NORMOKSIK JEL DOZIMETRE ILE INCELENMESI

Bu çalismadaki ana hedef Gamma Biçagi tedavisinde doku inhomojeniteleri yakinlarinda olusan doz dagilimini normoksik polimer jel fantomlar ile 3 boyutlu incelemektir. Jel fantom isinlanmasinin ardindan MR ile görüntülenmekte ve bu görüntülerin yeniden islenmesi ile her noktadaki gerçek T_2 degeri ile o noktaya verilen doz hesaplanmaktadir. Insan kafasinda yer alan yumusak doku-hava inhomojeniteleri yakinlarinda, elektron dengesi olusamamasi nedeniyle, tüm kafa içi dokulari su esdegeri kabul eden tedavi planlama algoritmalari hatali doz dagilimi öngörebilmektedir. Bu problem fiziksel fantomlar ile simüle edildi. Birinci deneyde kulak içi hava boslugu, diger deneyde ise sinüs hava boslugu yakinlarindaki bölgelere verilen dozlarin bu hava bosluklarindan etkilenmeleri ve dagilimlari arastirilmistir. Kulak boslugunun çalisildigi deneyde, cam balon içine hava bosluklarini temsil eden iki sise mantari uçlara yerlestirilmistir. Sinüslerin çalisildigi deneyde ise maksimal sinüslere benzesim yapacak boyutlarda bir mantar ile homojen olmayan fantom olusturulmustur. Her iki deneyde de içi MAGIC polimer jel ile doldurulmus 16 cm çapindaki cam balonlar, homojen fantom olarak kullanilmistir. Her biri 100 ml. hacimli plastik siselere doldurulmus jeller belirli dozlar ile isinlanarak doz-R_2 kalibrasyon egrisi elde edilmistir. Deneylerde homojen ve homojen olmayan fantomlarda ayni koordinattaki noktalara tek bir atislik doz verilmis ve olusan doz dagilim haritalari hesaplanmistir. Doz kalite kontrolü açisindan, Gamma Biçagi Planlama Sisteminin hesapladigi doz dagilimi ile deneysel sonuçlar karsilastirilmistir. Homojen fantom için gel dozimetrenin hesapladigi doz dagilimi ile GammaPlan'in hesapladigi doz dagilimi birbirleri ile uyum içindedir. Ancak homojen olmayan fantomda doz dagilimi uzaysal olarak farklidir ve degisik doz seviyeleri gözlemlenmistir. Yumusak doku-hava arayüzüne yakin bölgelerdeki dozun hizli azalmasi, bizleri GammaPlan'in bölgesel olarak fazla doz hesapladigi sonucuna götürmektedir. Kulak içi hava boslugu deneyinde homojen ve homojen olmayan fantomlarda olusan doz dagilimlarinda, aksiyel eksen Z=105 mm düzleminde %50'lik izodoz egrilerinin çaplari X ekseni boyunca %35, Y ekseni boyunca % 1; yine koronal eksen Y=105 düzleminde ise X eksen boyunca %39 ve Z ekseni boyunca %5'lik fark göstermistir. Paranosal Sinüs boslugu deneyinde ise homojen ve homojen olmayan fantomlarda Z=71, 75 ve 79 mm'lerde yer alan aksiyel düzlemlerde %50'lik izodoz egrilerinin X ve Y eksenleri boyuncaki çaplari sirasiyla %42 ve %47; %42 ve %60 ve de %52 ve %70'lik farklar göstermistir. GammaPlan'in bazi lezyonlarin arkasinda veya yakinlarindaki hava bosluklari yakininda olusan ani doz düsümünü hesaplayamamasi, gerçekte verilen dozun daha fazla olarak hesaplanmasina neden olmaktadir. Bu da insan kafasinda doku inhomojeniteleri yakinlarindaki lezyonlara gerekendenden az doz verilmesi dolayisiyla lezyon kontrolünü azaltabilmektedir.

Anahtar Sözcükler: Polimer jel, Jel dozimetre, Doz dagilimi, Doku Inhomojenitesi, Stereotaktik Radyo-cerrahi, Gamma Biçagi.

TABLE OF CONTENTS

LIST OF TABLES

LIST OF FIGURES

LIST OF ABBREVIATIONS

MR	Magnetic Resonance
CT	Computed Tomography

1. INTRODUCTION

1.1 Motivation and Objectives

The primary objective of this study is to appraise the spatial and relative dosimetric uncertainties of the radiosurgery procedure near areas of tissue inhomogeneities in the Leksell Gamma Knife Treatment planning by using the new normoxic Polymer Gel. Three-dimensional dose distribution in Gamma Knife Radiosurgery is anatomized by physical experiments using homogeneous and inhomogeneous normoxic polymer gel phantoms. The accuracy and precision of the Leksell GammaPlan, the dose planning system used in Gamma Knife Model-B, near the tissue inhomogenities is evaluated using the gel dosimetry methods. The normoxic polymer gel dosimetry is employed to calculate the dose distribution in the axial plane along the Z axis in one experiment and in three axes in the other experiment when a single shot, with 201 open Cobalt sources, is delivered to a known point with the same coordinates in the homogeneous and heterogeneous phantoms. In the view of dosimetrical quality control, the dose distribution predicted by the GammaPlan is compared with the MR calculated results. This is critical for target dose homogeneity, amount of dose delivery to surrounding normal tissues, and planning and optimization processes. The results will help in more accurate dose estimations for tumor control and sparing the normal tissue.

1.2 Overview of the Study

Stereotactic radiosurgery using the Leksell Gamma Knife is a treatment method of delivering a high dose of irradiation based on the principles of the Leksell Stereotaxy to a small and usually critically located intra-cranial volume through the intact skull in a single

session. Gamma Knife was invented and developed by Professor Lars Leksell from Karolinska Institute, Sweden. Leksell Gamma Knife is used for treatment of vascular malformations, benign tumors, metastases and other malignant tumors, as well as functional disorders. More than 250,000 patients around the world have received Gamma Knife surgery and each year more than 30,000 patients undergo this treatment. Non-invasive Gamma Knife radiosurgery assures the irradiation of precisely defined intracranial targets by a sharp dose gradient and high dose external irradiation from 201 small Cobalt 60 sources while minimizing the risk of damaging healthy tissue. Two hundred and one (201) beams of gamma radiation are focused to the targeted lesion with an accuracy of better than 0.3 mm as verified during the machine installation and periodical controls. Some of the Cobalt sources can be plugged to protect sensitive and vital organs from receiving high radiation. The age, number and locations of the Cobalt sources and the collimator helmet type used determine the dose distribution in the patient's head, and the collimator helmets used in the session. Standard collimator sizes are 4, 8, 14, and 18 mm, which size the treatment shots [1].

Leksell GammaPlan is a computerized dose planning system particularly devised for the Gamma Knife radiosurgery, which can exploit CT, MR-scans, or angiographic images. The lesions are identified on the images transferred to the GammaPlan. The dose distribution in the volume of interest is calculated using a mathematical formula in the GammaPlan. The inverse square law, linear attenuation exponential formula and single beam profiles for different helmets define the dose contribution conducted from a single beam. Superposition of dose contributions from 201 gamma beams is utilized to calculate the dose at any point within the patient's skull [2, 3].

Stereotactic Radiosurgery has two main objectives: (a) Precise stereotactic and geometrical definition of the target; (b) Precise delivery of the intended treatment dose to the target and minimizing dose to surrounding healthy tissue.

Due to its geometrical construction and small beam characteristics, Gamma Knife, creates highly complex dose distributions in three dimensions. The polymer gel dosimeter is a promising tool to measure the dose distribution of Gamma Knife in a three dimensional space. Polymer gel dosimetry is based on radiation-produced polymerization

and cross-linking of acrylic monomers in a gel matrix. The polymer concentration and the amount of the cross linking at any point in the gel are proportional to the delivered dose at that point. The polymerization and cross linking decreases T_1 and T_2 relaxation times of the neighboring water protons. By calculating the true T_1 or T_2 relaxation times in the gel, one can calculate the dose imparted to this particular point [3].

In recent years, the formulation for a new type of polymer gel, which can be produced and stored under normal atmospheric conditions, has been published. The gel is named MAGIC, (an acronym for Methacrylic acid, Ascorbic acid, Gelatin, Initiated by Copper). MAGIC is composed of distilled water, hydroquinone (18 mmol/l), Methacrylic acid (9%), and Ascorbic acid (2 mmol/l), Gelatin (8%), Copper Sulphate (CuSo4*5H2O), (0,02 mmol/l). This gel is called normoxic due to the fact that it can be manufactured and processed with contact to oxygen in air [4].

Polymer gel dosimetry has so far been employed in different radiation scenarios. However, little work has been reported investigating the dose distribution near an air cavity in a normoxic polymer phantom undergoing radiosurgery [5]. In this study, normoxic polymer gel dosimeter evaluated by MR imaging is used to calculate the dose distribution at the region near an air cavity under Gamma Knife treatment.

1.3 Outline

In chapter 2, dosimetrical uncertainties related to the Gamma Knife dosimetry near the tissue inhomogeneities are discussed. Stereotactic radiosurgery with Gamma Knife and stereotactic localization are explained. The physical and radiophysical characteristics of Gamma Knife are outlined.

Chapter 3 gives detailed information about the Gamma Knife treatment planning procedure. The algorithm of the GammaPlan is explained. The terms such as beam blocking, shot weight and output factors are defined.

Chapter 4 explains the principles of gel dosimetry. Normoxic polymer gel MAGIC is introduced and the radiation induced reactions are discussed. The characteristics of the MAGIC gel are presented.

Chapter 5 gives methods for manufacturing the normoxic gel and irradiation of the phantoms. The evaluation of the gel phantoms and calculation of true T_2 values are explained. The figures display the set up of the gel phantoms in the stereotactic frame and Gamma Knife.

In chapter 6 the results of the dose measurements are given in detail. The calculated diameters of the 70%, 50% and 30 % isodose curves are presented. The dose profiles in three axes are also illustrated.

2. Gamma Knife Treatment and Dosimetry of the Gamma Knife

2.1 Inhomogeneity Problem in Gamma Knife Radiosurgery

The treatment planning system of the Gamma Knife, the GammaPlan, ignores the tissue inhomogeneities by assuming all tissues and matter in the human head as being radiophysically equivalent to water under Gamma Knife irradiation. Treatment planning algorithms that assume all treatment volumes as homogeneous media equivalent to water, may fail to calculate the true absorbed dose in the vicinity of air-tissue inhomogeneity in the head, because of the absence of electronic equilibrium [6, 7].

In this study, homogeneous and inhomogeneous phantoms fabricated with normoxic polymer gel are used to investigate the effect of air-tissue inhomogeneity on dose perturbation during stereotactic surgery under the Gamma Knife.

2.2 Small Beam Dosimetry of the Gamma Knife

High-resolution dosimetry is an active topic in stereotactic radiosurgery and radiation therapy [8]. Gamma Knife radiosurgery is usually non-fractionated as opposed to radiotherapy. In order to inhibit side effects, tissue sparing is a key point, which must be achieved by delivering a much lower dose to normal tissue adjacent to the target lesion. Therefore, the accuracy of dose calculation is very important in stereotactic radiosurgery to satisfy this basic requirement [9, 10].

Dosimetry of narrow photon beams expresses some difficulties compared to conventional radiotherapy beams. The small dimensions and steep dose gradients of these beams require a detector with good spatial resolution. Due to the small size of the gamma beams, lateral electron equilibrium cannot be established around these beams, thereby

complicating the dosimetry. The contribution of secondary photons is also small, resulting in a different spectral distribution as compared with the large fields in which the detectors are normally calibrated [10, 11].

2.3 The Importance of Air Cavity Inhomogeneity

GammaPlan B uses a semi-empirical dose calculation methodology. The dose profile of each gamma beam is measured for collimator helmets of 4, 8, 14 and 18 mm. The dose distribution in the patient is calculated by superpositioning the dose distributions from all 201 gamma beams [2]. The assumption that the head is a uniform medium may result in undesirable effects when treating targets near air-tissue interfaces and may command alternative dose calculation methods [12, 13]. The goal of this study is to investigate the importance of air-tissue inhomogeneity in stereotactic radiosurgery with the Leksell Gamma Knife B.

In stereotactic radiosurgery, considering the patient head to be a homogeneous medium may be relevant in many instances, as in gliomas, metastatic tumors and arteriovenous vascular malformations (AVMs). However, when lesions are located near the air cavities, the dose distribution is affected by the combined effects of the decrease in attenuation, the decrease in photon scatter and the lack of electronic equilibrium in an air cavity. Rustgi et al have shown that air cavities and low-density inhomogenities near the nasopharyngeal and sinus regions produce a significant perturbation in the dose distribution for narrow 6 MV X rays near the inhomogeneity [14]. Solberg et al have investigated the narrow megavoltage beams with a diameter of 1–3 cm used in radiosurgery [12, 13, 14]. It has been shown that a lower dose is measured on the distal surface of the air cavity than would have been recorded in the uniform density case [15]. These results are significant, leading to inaccuracies in treatment planning. Dose reduction is reported to increase with air cavity thickness and field size. While electronic equilibrium is re-established, a secondary build up region is observed, and the dose after the build-up region is larger than the dose at the same depth in a uniform-density phantom [13]. A target immediately below the low-density inhomogeneity will thus get a lower

dose to a depth of 4–6 mm (d_{max} of secondary build-up for a 6 MV and Co-60 photon beams) and target volume with distances more than 6 mm will receive a higher dose than that predicted by a treatment planning system, which assumes a uniform-density medium. Another outcome of the air inhomogeneity is the increase in dose outside the beam geometric edge and a decrease in the dose inside the beam edge. Monte Carlo studies have simulated these same effects. However little work has been reported for investigating these effects experimentally in a three-dimensional phantom [12, 13, 14].

Cavernous sinus meningiomas are usually near the optic apparatus. Optic chiasm is a sensitive organ for radiation; therefore tumors around optic apparatus are given a lower dose than the standard protocol which is reported to yield difficulty in controlling the tumor growth. An example reported in a statistical study states that 14 Gy of dose can control the tumor growth in 100 % of the patients having cavernous haemangiomas. However, 20% of the patients who received a dose between 10 and 12 Gy have experienced tumor regrowth. Most of the recurrences or regrowth of cavernous sinus meningiomas were adjacently localized regions to the treatment site, which suggests an underdosing at the target's margin. Similar problems occurred for the treatment of cavernous haemangiomas in the cavernous sinus. The dose distributions near the sinuses are critical in controlling these tumors. Therefore, the clinical statistics suggest lesions near air-filled cavities in the head have still uncertainties in radio-surgery with the Leksell Gamma Knife B [1].

2.4 Stereotactic Radiosurgery and Gamma Knife

Brain tumors have indications like motion and sensory problems, headaches, vision problems, character changes, cognitive disorder, and hormonal abnormalities. Treatment of patients with brain tumors is a highly specialized area of neurosurgery and neuro-oncology [16]. Today, stereotactic radiosurgery is a main treatment modality in neurosurgery. This radiosurgery has been used primarily for intracranial tumors that are

not suitable for surgery. This technique is especially helpful for patients who cannot undergo an open brain surgery [17]. Radiosurgery is limited to tumors up to 4 cm in diameter and is remarkably useful in treating Arterio Venous Malformations (AVM). In recent years, research about fractionated stereotactic radiosurgery for treating larger tumors is ongoing [15].

Stereotactic radiosurgery is a treatment procedure used to treat brain tumors, AVMs and functional disorders. This procedure does not involve surgery and is non-invasive. In this technique, the dose delivered to the lesion can ascend to 10 times the regular doses in radiotherapy and is delivered in a single session of treatment [17]. Contrarily, almost all of the radiation therapy for brain lesions was fractionated before radiosurgery was invented [19].

In the earlier studies of radiosurgery, Dr. Leksell firstly combined a rigid immobilization and stereotactic targeting system with a single orthovoltage radiation beam. However, the energy from a conventional X ray tube was insufficient for the purposes of radiosurgery. Thereafter, he tested the synchrocyclotron to produce proton beams used for radiosurgery. The synchrocyclotron was an expensive device that many centers could not afford to purchase. Later he used a multiple beam technique with Co-60 sources to allow a sharper falloff dose to adjacent healthy tissue. Leksell used his technique in the brain, which is accepted as the most significant organ and least tolerant to the effects of radiation in the body. Moreover, he used a single session treatment; opposing the general thought that fractionation is better for radiation tolerance [19, 20].

Figure 2.1: The Gamma Knife Unit

2.5 How Stereotactic Surgery Treats

The radiophysical principle for stereotactic radiosurgery is similar to radiotherapy. The goal of radiosurgery is to control the tumor growth for the intracranial tumors and to eliminate the future risk of bleeding for the AVMs. Radiosurgery does not remove the tumor or tissue abnormality. For the intracranial tumors, radiation delivered demolishes the cells in the target tissue by damaging their genetic material (DNA). Radiation induces mutations and DNA malformations. Due to the ionization and DNA damages, cells stop growing and replicating and lose their ability to retain water. Tumor reduction occurs at the rate of the normal growth rate of the tumor. For metastatic tumors it takes about two months to disappear and for benign tumors it can take up to 2 years to disappear [21,22].

An Arterio Venous Malformation (AVM) is an abnormal cluster of blood vessels in the brain or spine. In the presence of AVM, the arteries pass the blood directly to the veins, bypassing the capillaries. The blood flowing through an AVM fails to carry oxygen

or nutrients to the brain or spinal cord and acts as a shunt. Stereotactic radiosurgery destroys the abnormal shunt vessels. Radiosurgery radiation induces the thickening and closing of the blood vessel. When the AVM is closed off, no more blood flows through and the patient is free from the risk for hemorrhage or stroke. The shrinking of a tumor or closing off a vessel occurs over a period of time [22].

2.6 Stereotactic Localization

Gamma Knife radiosurgery integrates the strengths of stereotaxy with converging beams of high energy radiation to distinctly irradiate an abnormal lesion within the patient's head. Four pins attach the stereotactic frame to the patient's skull. The frame stays in the patient's head until treatment is completed [23]. The patient's head is positioned so that the tumor is centered in the focus where all the beams intersect. Each beam passes rather safely through scalp, skull and the brain tissue. However beams focus on the lesion with a highly localized dose. Radiosurgery is totally non-invasive except for the application of a stereotactic frame [24].

Stereotaxy is a methodology of localizing structures in the brain with three-dimensional coordinates, based on the use diagnostic images and surgical instruments to contact these points. The word stereotactic comes from stereo meaning three dimensional and tactic meaning movement toward. Targeting with stereotactic localization is entirely different from the localization in radiotherapy. In radiotherapy, at least three skin marks are pointed to identify the beam's isocenter. This point is placed to match the geometric center of the tumor. Therefore, all beams are directed toward the tumor by virtue of at least three skin marks often referenced to a bone. Since skin and bones are flexible and movable structures, any deviation for the reference points results in unsuccessful direction of the beam toward the target. However, in stereotactic localization, three dimensional coordinates are assigned to any point in a volume of interest. These coordinates are referenced by the coordinate system on the axes of the head frame [21, 25].

2.7 Stereotactic Radiosurgery Systems

The three common modalities used for stereotactic radiosurgery are the Gamma Knife, modified linear accelerators and charged particle accelerators such as proton beam accelerators [24]. The Gamma Knife treatment unit is very robust since it has no moving parts except the patient couch and submits a reliable beam profile. A significant advantage of the Gamma Knife is that it can create rather conformal treatment plans by using multiple shots, which is advantageous in treating near the brainstem and cranial nerves [18, 26, 27].

2.8 Differences Between Stereotactic Radiosurgery and Radiotherapy

Stereotactic radiosurgery is different from conventional radiotherapy in many aspects. The principle of radiotherapy is based on the greater susceptibility of tumor cells to radiation compared to normal tissue cells. The spatial accuracy on the target is of secondary concern because the fractionation to several weeks and irradiating a margin near the tumor boundary is helpful for tumor control in radiotherapy practice. In stereotactic radiosurgery normal tissues are protected by the rapid dose decrease outside the target region and also the deployment of converging beams to minimize the dose to the tissue in the path through the target [24].

Due to the requirement of organ immobilization for the accurate treatment, stereotactic radiosurgery is restricted to the head and neck. Delivering a high dose in a one day treatment without a skeletal fixation device is not acceptable because of the high possibility of damaging healthy brain tissue, cranial nerves such as optic, hearing nerves and the brain stem [17, 28].

Figure 2.3: Stereotactic Frame with the fiducial markers attached to the head of the patient

Figure 2.2: The fixation of the stereotactic frame on the patient's head before the treatment

Figure 2.4: The patient entering the Gamma Knife treatment

Stereotactic radiosurgery is generally used to treat lesions in the range of 5 mm to 40 mm in diameter, while radiotherapy fields can be up to 400 mm [20, 24]. Radiosurgery requires spatial accuracy of about 1 mm and an uncertainty of no more than 5% in order to conform the dose to the target volume. The spatial accuracy of Gamma Knife in the Marmara University Hospital was found to be approximately 0.25 mm. Mechanical accuracy should be less than 0.3 mm according to manufacturer's specifications.

2.9 Physical Description of the Gamma Knife

There are currently three versions of the Leksell Gamma Knife (Models U, B, and C, Elekta Instruments, Atlanta, GA). The model B unit was presented in Europe and Asia and was approved by the Food and Drug Administration for use in the United States in 1996. The Model C unit having a robotic positioning system was presented in 2000 [29].

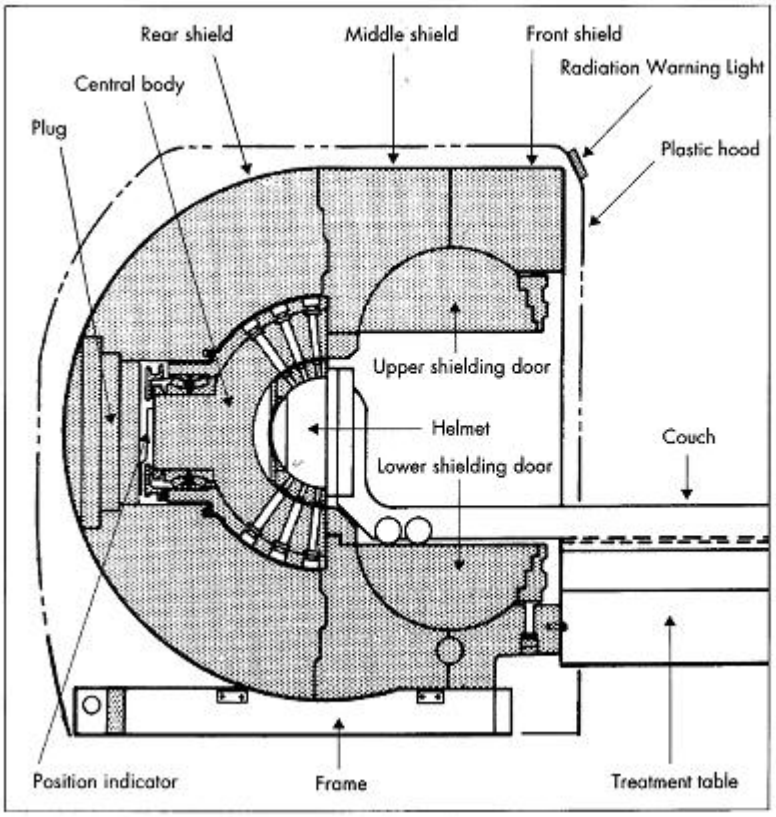

Figure 2.5: The physical structure of the Gamma Knife

The physical appearance and structure of the three models are different. However, the radiation delivery system of each is designed to produce similar dose profiles. Each model consists of six components: the radiation unit, the collimator, the patient couch, hydraulic bed system, the control console, and the treatment planning computer system [27]. The radiation unit has a central body housing Co-60 sources with collimators, a shielding door and is covered by 18,000-kilogram cast iron shield. The hemispherical

shield at the top of the unit has a radius of 82.5 cm and is 40 cm thick. The hemispherical central body fits closely into the inner radius of the upper shield [2, 3].

2.10 Cobalt Source Assembly.

Cobalt 60 sources are placed in a circular array and distributed evenly in an arc of +/- 48^0 along and +/- 80^0 across the treatment table from the central beam. No primary beam of radiation is directed out of the hemispherical shield or the shielding door. Each source consists of twenty 1-mm diameter pellets stacked on one another. They are encapsulated doubly in stainless steel capsules and produce a very small penumbra at the intersection point. Each beam channel has source bushing assembly, a thick tungsten alloy pre-collimator, and a lead collimator. The focal distances of the collimator helmets are 40.3 cm. The central beam of the 201 source array lies at a fixed angle of 55^0 to the horizontal plane. The beam from each individual cobalt source is delivered through a device known as the collimator helmet, which is fixed to the patient's head by special screws. Cobalt sources are approximately 30 curies during the installation. A dose of 5,000 cGy could be delivered within 20 minutes, to a tumor [3, 20].

2.11 Collimator Helmets.

The final collimation is accomplished by one of the four helmets. Each helmet is 22.5 cm in diameter and is of a 6-cm thick cast iron shield. 201 channels have been drilled to house 4-, 8-, 14-, or 18-mm tungsten collimators with circular apertures that create certain size fields at the focus. Any of the removable collimators can be replaced with an occlusive plug to prevent irradiation of the lens of the eye or other critical structures near the target [2, 20].

The hydraulic system controls the opening and closing of the steel door and movement of the patient couch in and out of the radiation unit. In a power failure, the reserve hydraulic pressure automatically releases the treatment table and closes the shielding door for safety reasons [2].

Figure 2.6: The collimator helmets of the Gamma Knife

Figure 2.7: The Control Console of the Gamma Knife

Figure 2.8: The GammaPlan

2.12 Control Console And The Hydraulic System.

The control console has a primary and a back-up timer. An infrared camera and a monitor show the inside of the treatment room. The console is equipped with a diaphone system for communicating with the patient [2].

2.13 Volume treated in Gamma Knife Irradiation

Gamma Knife performs treatments of the smallest volume, which is 1 cm. According to the smallest lesion size treated in Gamma Knife, a geometrical accuracy and precision of less than ± 0.5 mm is required. The most robust way to achieve this is to keep

radiation delivering systems motionless during the course of treatment. Additionally, beam shaping parts should be designed to produce narrow beam size [31].

However, there is a limit for the largest size of lesion to be treated by the Gamma Knife. Figure 2.9 shows the instance in two dimensions when a small size target is irradiated with narrow beams. Figure 2.10 shows a large target irradiated by broader beams:

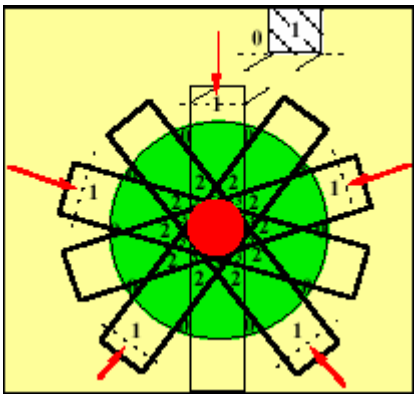

Figure 2.10: The target shooting with broader beams [31].

Assuming the dose delivered in the section inside the beam as 1 and as 0 outside the beam, we can recognize the penumbral effects in Gamma Knife irradiation. In this simulation, only geometrical and spatial factors are considered while neglecting the attenuation, inverse square law or particle scattering. In the second case, broader beams irradiating the larger target begin to superimpose further from the target border. As a result, considerably larger volume of normal tissue receives therapeutic dose. This simulation expresses that radiobiological factors limit the largest size of the target volume that can be treated by the Gamma Knife radiation [31].

2.14 Gamma Knife Precision and Accuracy

When we study the volume of beam intersection closer, we see that the beam axes do not cross exactly at one single point in the Gamma Knife (Figure 2.12). This beam misalignment has two effects on quality assurance: First, the isocenter can be shifted from the predicted coordinates, which is a geometrical error. Second, the dose distribution may also differ from the presumed; that is, the dose is spread over a larger region and its magnitude can be less than calculated [31].

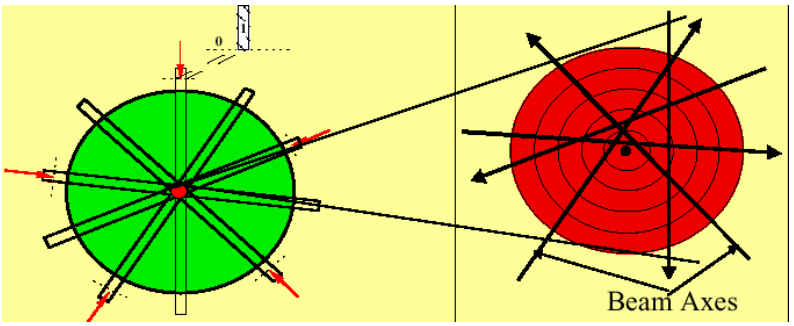

Figure 2.11: The off axis characteristic of the Gamma Knife irradiation [31].

The errors should be checked during the Quality Assurance checks and are tolerable up to a limit. The center of the smallest sphere through which all beam axes pass is the radiological Unit Center Point (UCP) or isocenter (Figure 2.12). The radius of this sphere can be seen as a measure of the spread of the beam axes or the uncertainty of their location. This uncertainty is called “the precision of the Gamma Knife” [31].

In order to measure the precision of the Gamma Knife, measured dose profiles are compared with the calculated dose profiles in GammaPlan. The used tolerance is ± 0.5 mm for the present. A spherical phantom simulating a human head is used for the film exposure. The films are placed in a special cassette holder at the center of the sphere and the sphere can be rotated to orient the film to the three axes. The distance between the

mechanically defined Unit Center Point and the one defined by radiological means is called “The Gamma Knife Accuracy”[31].

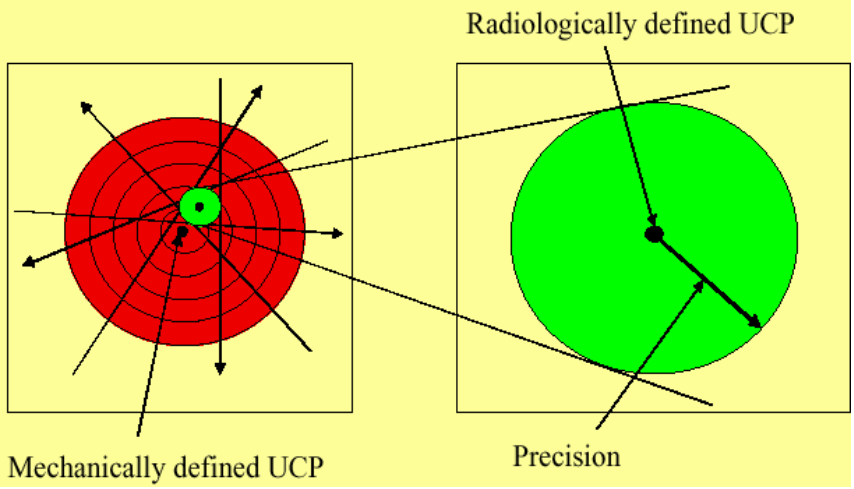

Figure 2.12: The mechanically and radiologically defined isocenters of the Gamma Knife [53].

2.15 Timer Correction

Unlike the Co-60 source in a teletherapy unit, the 201 Cobalt sources in the Gamma Knife do not travel. The gamma knife exposes a small transit dose during the helmet’s entry and the exit from the focus. Therefore, the timer is adjusted to account for the transit dose [32].

2.16 Radio-surgical Procedure

The patient, whose head is fixed in the stereotactic head frame, is placed on the couch of the Gamma Knife. The determined X, Y and Z coordinates of the shot are adjusted by the physicist or the technologist. The Y and Z coordinates are set on the adjustable side pillar of the frame and the x coordinate is set by fixing the frame to the collimator helmet. The appropriate collimator helmet is chosen and fastened to the head of the couch. The patient's head is then fixed to the inside of the collimator helmet by means of the head frame. The radiation time is set in the control unit. The personnel leave the treatment room and the lead hardened door of the treatment room is closed. The neurosurgeon pushes a button to start the treatment [33].

When the start button is pushed, the doors on the Gamma Knife open. The couch with helmet and the patient are then pulled into the Gamma Knife. The collimator helmet locks into proposed place and a timer starts counting. When the prescribed time for the irradiation is reached, the couch with collimator helmet and patient is automatically pulled out of the unit and the Gamma Knife doors close [33].

Adjustments for the other planned shots are done afterwards. The patient is detached from the collimator helmet and new X, Y and Z coordinates are set on the stereotactic frame. The collimator helmet can be replaced with another collimator helmet of a different size. The irradiation process begins again [33].

3. TREATMENT PLANNING IN GAMMA KNIFE RADIOSURGERY

3.1 Imaging Techniques and Target Localization

In order to obtain images for treatment planning, different imaging modalities are used according to the type of lesion. Computed Tomography (CT) or Magnetic Resonance (MR) imaging is usually used for tumors such as acoustic neuromas, pituitary adenomas, and other cerebral neoplasms. For AVMs, usually angiographic images of the brain are used [2, 20].

The images from CT, MR or angiography are transferred to the GammaPlan. The frame's rectilinear fiducial markers can be seen on the images. The markers are used to find the three-dimensional coordinates and to match the magnification factor of the images in the space of the frame. The center of the frame is set to X=100, Y=100, and Z=100. X, Y, and Z coordinates of points in the target are derived from the images [2, 34].

3.2 Derivation of the Skull Shape

A purpose-built plastic helmet is attached to the stereotactic frame to measure the distances from the center of the stereotactic frame to the 24 pre-selected points on the skull. The GammaPlan uses these distances to create a 3-dimensional simulation of the skull. This model is used to construct the skull in treatment planning rather than the diagnostic images. A 31x31x31 point matrix centered on the region of interest is created inside which the dose is calculated for all the points. The size of the matrix depends on the grid size chosen which can be varied from 0.1 to 2.5 mm. The dose distributions are normalized with respect to an absolute dose at a given point [2, 35].

Figure 3.1: The plastic helmet attached to the patients head to determine the skull shape

3.3 Dose Calculation with the Planning Algorithm

The hardware for the treatment-planning computer system is composed of a computer, two monitors, one for the command line and the other for graphics, a plotter, and a printer. Using the predicted target coordinates and the size of the collimator of each shot, GammaPlan calculates and displays the isodose distributions in the three principal planes X-Y (axial plane), X-Z (coronal plane), and Y-Z (sagittal plane); and then superimpose on the radiographical images (CT, MR etc) [23, 29].

There are some dosimetric parameters that are used to calculate the dose distribution. The customer sets the dose rate at the center of the spherical phantom for the 18 mm helmet, with all 201 sources opened and by measuring the dose with an ion chamber or diode detector. The relative output factors for 4, 8 and 14 mm helmets, the

radial dose distribution of a single-beam at a focal distance of 400 mm and at a depth of 80 mm in water for all helmets, and the linear attenuation coefficient of Co-60 beams are pre-stored in the LGP [36].

In the GammaPlan algorithm, dose distributions from 201 gamma beams are superimposed to calculate the dose at any location inside the patient's skull. The dose submitted from a single beam depends on the skull shape, the inverse square law, the linear attenuation of gamma beams in the skull, dose profiles for different collimator helmets pre-stored in the GammaPlan and the dose reference point in a tissue equivalent phantom [2, 36].

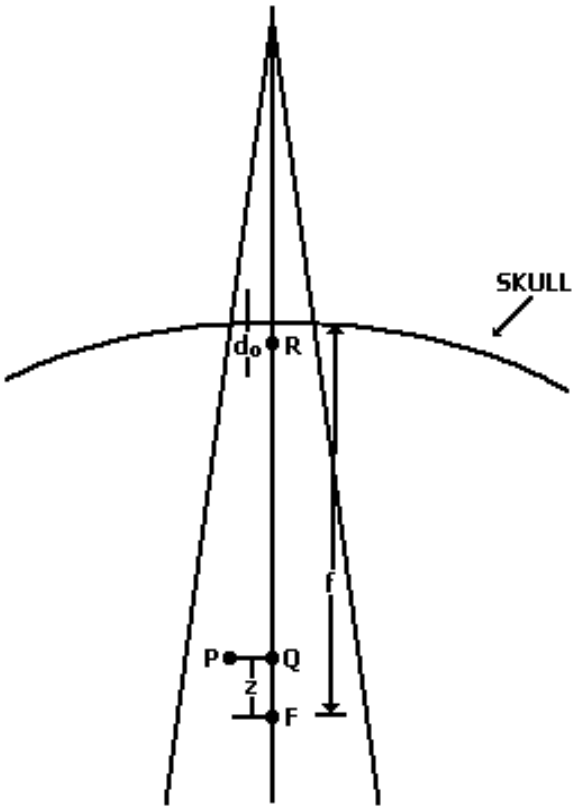

Figure 3.2: Dose calculation of GammaPlan at any point in the skull.

Figure 3.2 illustrates the GammaPlan dose calculation algorithm: The distance between any Cobalt-60 source (S) and the focus (F) is 40,3 cm. A point at depth, d_o, which is 1 cm from the surface of an 8 cm radius phantom, is assigned to be the reference point

(R). The manufacturer has measured the dose conducted from an individual source Cobalt-60 for a certain collimator helmet at the calibration at the reference point R [2].

For any point P inside the tissue equivalent phantom, point Q is defined as the point at the same depth as point P in the central axis of the beam. The distance |QF| between point Q and the focus F is defined as z. The distance |SR| between the source S and reference point R is 33.3 cm. Again the distance |SQ| between the source S and point Q is (40.3 cm - z). The manufacturer provides the dose at the reference point R. Knowing the distance between the source and the reference point as 33.3 cm and the distance |SQ| as (40.3 cm - z); the dose at the point Q can be calculated using the inverse square law and linear attenuation formula. Thereafter, the dose at the point P from an individual beam can be calculated by the off-axis-ratio, which is obtained from dose profile [2,3].

3.4 The Treatment Goals

The typical treatment goals in a stereotactic radiosurgery planning are:

1. Homogeneity, which requires the coverage of the lesion usually by the selected isodose curve for tumor damage. The main objective in stereotactic radio-surgery planning is that a certain isodose line covers the target volume and that dose to neighboring normal tissues is minimized. The dose gradient from the 50% isodose to the 30% isodose lines is important forming a shell dose in the borderline of the target region, within a distance of 2 to 4 mm [36].

2. Conformity, which requires the minimization of healthy tissue covered by the delivered shots. This helps in the risk reduction and success in cell recovery.

3. Organ avoidance, which requires minimization of dose to certain critical structures in the skull, which is essential not to damage certain brain and nervous functionalities.

3.5 Art of Treatment Planning

Radio-surgery planning is usually a multidisciplinary procedure contributed by specialists in Neurological Surgery and Radiation Oncology [24]. The neurosurgeon, the radiation oncologist and the radiation physicist work on the dose distribution plans by using the different collimator helmet sizes and shots. A shot is one session of treatment delivering an almost spherical volume of dose. In a typical treatment, multiple shots of different sizes and durations are centered at different points of the tumor. The treatment time for each shot is dependent on factors such as the weight attributed to the shot, the relative output factor of the selected helmet, and the output of the unit at the focus for the particular skull shape. Conventionally, the tumor dose is prescribed to the 50% isodose curve with 100% normalization to the maximum dose. The GammaPlan adds the dose delivered from the proposed shots and illustrates a radiation dose field, which is supposed to represent the same shape as the lesion. When such a suitably shaped dose volume is reached with a method of trial and error, the GammaPlan specifies the stereotactic coordinates for each shot and the shot duration. Thereby, the treatment planning process determines the center and durations of the shots and which of the collimator helmets to shape the beam. The planning of the tumor is dependent on the size, shape and the location. When a tumor is small enough it can be irradiated by one shot. On the contrary, if the tumor is larger or is far from spherical or elliptical shape then multiple shots is needed to cover the tumor to the selected isodose curve[37,38] .

Hypothetically, the neurosurgeon can use any number of shots for the radio-surgery, however the time for the planning and irradiation setup for more than five shots is not practical. The relative weighting must be specified for each shot [37].

3.6 Shot Weight

Shot weight specifies the amount of dose attributed to a single shot using a definite collimator helmet. As the shot weight increases, the intensity of the dose profile increases as well. This enlarges the shot diameter. Therefore as the shot weight increases, the profile width at a given absolute dose increases as well. Shot weighting acts as a useful tool in placing the 50% isodose line into the border of the tumor [36].

3.7 Blocking

Beam blocking is another feature of the GammaPlan. Blocking is used for protecting the sensitive structures such as the optic chiasm, lens of the eye, brainstem and facial nerves in addition as a shaping tool for the overall dose distribution. Blocking is performed using occlusive plugs that replace collimator apertures for each collimator helmet [36].

3.8 Beam Data Stored In Gamma Plan

The beam delivery system of the Gamma Knife is designed to minimize the variances amongst the beam. Hence, the beam channels are constructed with very small tolerances to be specified as identical mechanically and radiophysically which markedly simplifies the storage of beam data in the GammaPlan. Therefore, some parameters stored in the GammaPlan entered by the manufacturer are measured during the laboratory installation and trusted for all the Gamma Knife sites [31].

The radiophysical data pre-stored in Gamma Plan are:

1. The four beam profiles shaped by each collimator helmet, measured at a distance of 400 mm from source and at depth of 80 mm in polystyrene phantom
2. Data set to calculate Percentage Depth Dose
3. Four measured Output Factors of the collimator helmets [31].

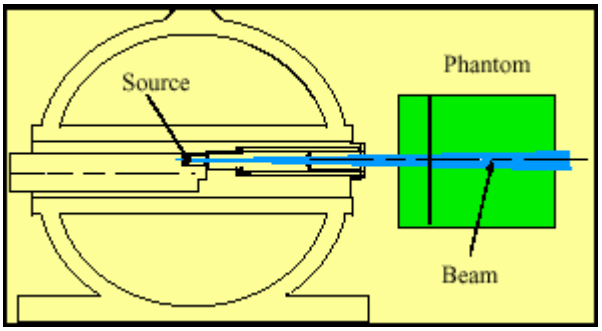

Figure 3.3: The experimental beam channel in the measurement of the beam profiles [31].

In the acceptance tests of the Gamma Knife, the dose profiles (at the sphere center and in the case of multibeam geometry) calculated by the GammaPlan are verified as part of the Gamma Knife acceptance test using silver halide film densitometry; the measured profiles are consistent with the computer generated data [31].

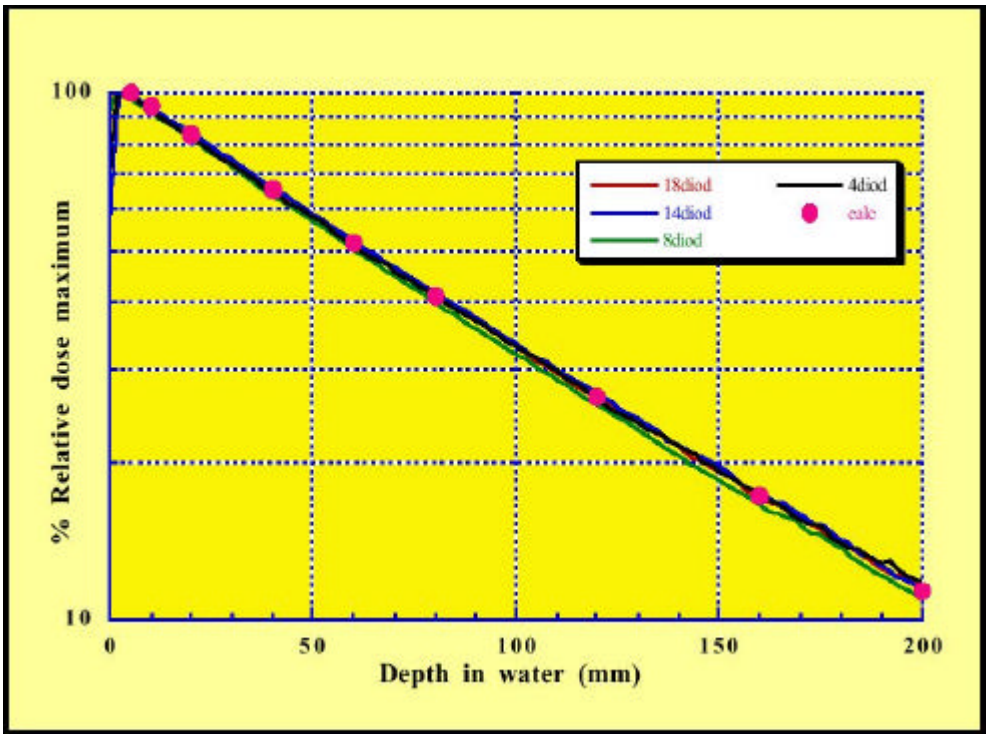

Figure 3.4: Percentage Depth Dose data for Gamma Knife [31].

The change of the attenuation coefficient for different beam sizes is small in the Gamma Knife. The inverse square law plays a dominant role in the percentage depth dose measurements [31].

3.9 Output Factors

The relative helmet factor (output factor) is defined as the ratio of the dose rate of all four collimator helmets to that of the 18-mm helmet. By knowing the output factors and the dose rate of the 18-mm collimator helmet, the dose-rate could be calculated for the other helmets [31].

The old recommended output factors of the 14, 8 and 4 mm collimators were 0.984, 0.956 and 0.800 respectively [41]. The most uncertainty is involved in measuring the

output factor of the 4 mm because of the smallest beam size, the size of the sensitive volume of the detectors and their alignment. Numerical values between 0.63 and 0.93 have been reported to be the two most common errors [39].

4. GEL DOSIMETRY

4.1 Background of Gel Dosimetry

In the new conformal radiation treatment techniques like Intensity Modulated Radiation Therapy (IMRT), High Dose Rate Brachytherapy (HDRB) or Stereotactic Radiosurgery (SRS), verifying the treatment plans is utmost importance. These treatment modalities require the knowledge of the three dimensional dose distributions as the outcome of the prescribed radiation plans [40].

The system primarily used to measure the dose in three dimensions is the water phantom with a movable radiation detector. Dose measurement in a volume is cumbersome with the point detectors. Additionally, this system is not competent to measure dose created by multiple sources. Film dosimetry is able to measure the dose in two dimensions whereas the direction of beams affects the image. Gel dosimeter is an appropriate nominee to measure dose in three dimensions [8].

The working principle of the chemical dosimeters is that products of radio-chemical reactions are related to the delivered dose at any point in the dosimeter. Gel dosimeters are chemical dosimeters where the gel material fixes the radiosensitive chemicals, chemical products, and the radicals by reducing their diffusion [41].

Day and Stein investigated gels containing Folin's phenol in 1950 changing color when irradiated. Later, Andrews et al measured photon and electron depth doses were in agarose gels. One of the first gel dosimeter was developed in 1957, in which chloral hydrate was utilized as the radiosensitive chemical. The product was HCL in the result of radiochemical reactions and the amount of the amount of HCL could be measured by the use of the electrical resistivity, pH or Cl^- analyses. Likewise dyes are used as a chemical dosimeter due to the change of their color under radiation. As an example, Xylenol

Orange dye changes color when irradiated which makes it suitable for optical scanning [41,44].

4.2 Fricke Gels

Gore et al proposed the analysis of the gel dosimeter using magnetic resonance imaging in 1984 [42]. The procedure involved the use of Fricke ferrous sulphate chemical dosimeter solution in gelatin. This kind of gels was called Fricke gels. When Fricke gels are irradiated, Fe^{+2} ions in the dosimeter gel change into Fe^{+3} ions. This conversion alters the magnetic dipole moments of the of the hydrogen nuclei in the gel, which can readily be detected as a change in the true T_1 and T_2 relaxation times by the use of MRI [42, 43].

Fricke gels have been deployed in Stereotactic Radiosurgery, Orthovoltage X-Rays, Linac Radiosurgery, brachytherapy and various Radiotherapy applications [41, 42].

The major disadvantage of Fricke gels is the immediate diffusion of the ferric ions and hence the loss of data related to the dose distribution. This yields blurring of the dose distribution in the dose maps [42, 43]. Accordingly, Fricke gels are suggested to be scanned in two hours after irradiation. The diffusion of ferric and ferrous ions enforces the use of fast T_1 imaging. The diffusion coefficients of the ions in the gel were investigated in various studies [42, 45].

Initially, the Fricke gel was used in the experiments. However, the results were unsatisfactory. Therefore, the normoxic polymer gel was preferred due to its ease of use, and since the diffusion of chemical products is not a problem as in the Fricke gels.

4.3 Polymer Gels

The diffusion problem in Fricke gels has led the development of a new kind of gel dosimetry system. In 1958, Hoecker and Watkins built the first polymer gel. Polymer gels are made up of the active components, the monomers inserted in a gelatin matrix. When irradiated, various radicals are induced in water, which initiate a polymerization reaction through cross linking of monomers [41].

Polymer gels are basically hydrogels, which can absorb large amounts of water without melting in it. Due to the cross linking of the hydrophilic polymers, polymer gels consists nearly 90% of water. Methacrylates and methacrylamide are the most commonly used monomers [46].

Polymer gel is conventionally employed in biochemistry as a medium for electrophoresis of protein and nucleic acid separation. In electrophoresis, the polymerization is generally launched by a free radical like ammonium persulphate. In radiation therapy polymerization is initiated by free radicals as the products of water radiolysis upon radiation. Near the polymerized area, water molecules alter binding to and interchange protons with the polymer structure [47].

The amount of polymerization is proportional to the delivered dose and the final polymer structure takes the shape of spherical polymer aggregates [49]. The aggregates decrease the mobility of the neighboring water molecules, which can be detected as a decrease in T_1 and T_2 relaxation times of the protons in water molecules. MRI has been the most widely used method for measuring the absorbed dose in polymer gels [40, 48]. True T_2 measurements were found to be less noisy and are usually preferred over the true T_1 calculations [49, 50]. The dose distribution can be calculated and constructed by deriving an R2 ($1/T_2$) map from a set of T_2 weighted images. The change in R_2 is proportional to the dose delivered in polymer gels. The objective of dose accuracy in gel dosimetry has been reported to be 3%[51].

The diffusion of the polymers is negligible in the gel matrix. Therefore, the data integrity problem as a result of the diffusion of ions in the Fricke gel is not encountered in the polymer gels. Accordingly, the dose distribution pattern is preserved for weeks after the irradiation. In the early developed polymer gels, acrylamide and the cross linker monomer N, N-methylene bisacrylamide were used. Polymer gels involving acrylamide are called PAG or BANG-1 R (BANG is the trademark of MGS Research Inc.) in the literature. The polymer gel dosimeters BANG-2 R and BANG-3 R contain the monomers acrylic acid and methacrylic acid, respectively [55,47]. Several studies have been done to investigate the dose sensitivity of different compositions and the physicochemical reactions that occur in the dosimeter gel during and after irradiation. [52].

Early polymer gels had the disadvantage of requiring hypoxic conditions for manufacturing and storage. For this reason, glove boxes were used and gel solutions were bubbled with nitrogen to remove the oxygen in the gel. Oxygen is an inhibitor for the polymerization. Since the bis and acrylamide used in the polymer gels are neuro-toxic, and can easily be absorbed through the skin or by inhalation, gels using acrylic acid and methacrylic acid have been developed [53].

The gels produced with gelatin are clearer for optical imaging techniques compared to the ones produced with agarose. Water protons in gelatin systems also have lower R_2 values than those in agarose gels. This decreases the baseline R_2 enhancing the sensitivity [46]. The melting point of the gel increases with the strength of the gelatin. 300 bloom gelatin is usually employed with a comparatively higher melting point as 30-35 ^{0} C. However, R_2 and gel sensitivity decreases when the gelatin concentration increases. Therefore, usually gelatin is used with a concentration of %5 by weight [54].

Though polymer gels have been validated in several studies, their use in the routine clinic has been restricted. The main reason is the strenuous manufacturing procedure including the avoidance of oxygen [5].

4.4 Evaluation Techniques for Gel Dosimeters

MRI, X-ray Computed Tomography, ultrasound, vibration spectroscopy and optical scanning are the methods used for measuring the polymerization in polymer gels [53,56]. Polymer gels become visually opaque when irradiated and change their optical characteristics that can be detected by optical imaging techniques [57].

X-ray CT is used to measure the change in the attenuation of the gel as a result of the polymerization. Polymerization changes the elasticity of the medium, which changes the velocity and absorbance of sound in the medium. This enables determining the dose distribution using ultrasound. Changes in the MR spectrum of polymer gels enable to obtain dose distribution by proton spectroscopic imaging [8].

4.5 Normoxic Polymer Gels

Fong et have developed a new kind of polymer gel named MAGIC, which could be manufactured, stored and used under normal atmospheric conditions without additional effort to avoid oxygen [54]. MAGIC is an acronym for Methacrylic and Ascorbic acid in Gelatin Initiated by Copper. In MAGIC gel, 300 bloom gelatin is used as the gelling material, methacrylic acid is the monomer, and distilled water is the solvent. The anti-oxidant materials in the gel enable this normoxic gel characteristic. Oxygen is expelled from the gel by the anti-oxidant [53].

Because of their ease of use, MAGIC gels have been utilized in many applications in the conventional radiotherapy and modern conformal techniques such as stereotactic radiosurgery, IMRT and high dose rate brachytheraphy [55, 56]. Though minor oxygen

effects may still be experienced, normoxic gels are very encouraging as gel dosimeters [46, 49]. . The radiation response of MAGIC has been found to be linear up to 30 Gy [5]

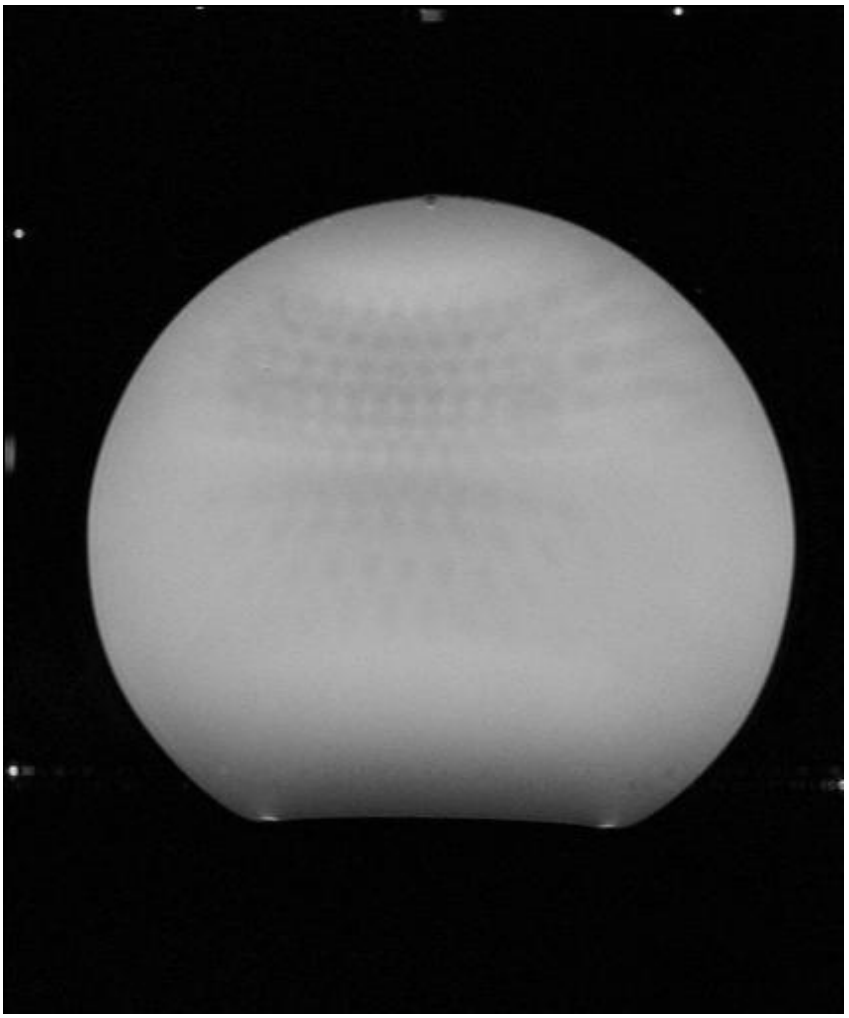

Figure 4.1: The 201 Cobalt sources silhouette image is visible in the localization MR image of the homogeneous phantom.

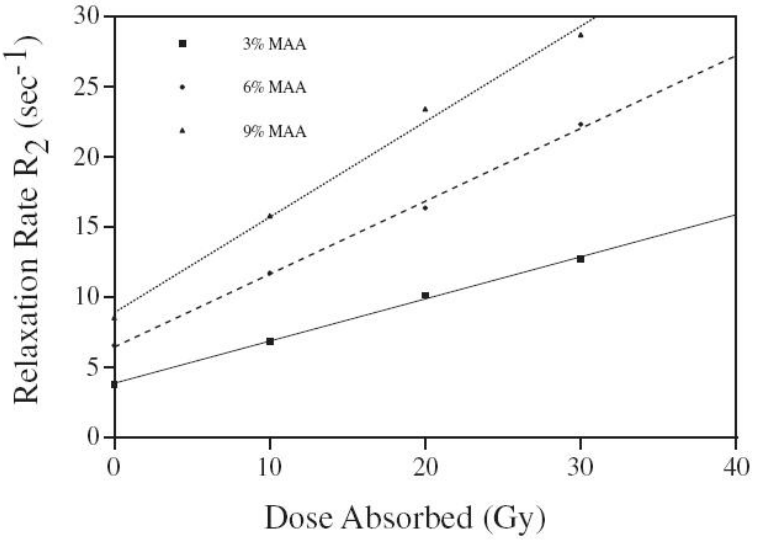

Figure 4.2: Dose response curve for 3,6 and 9 % Methacrylic acid MAGIC gels: R_2 (1/s) versus dose (Gy) at 85 MHz [5]

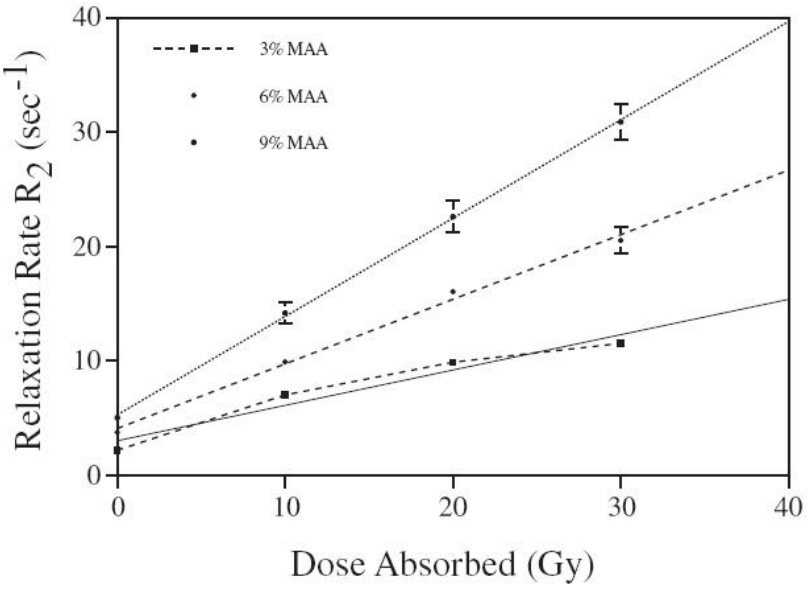

Figure 4.3: Dose response curve for 3, 6 and 9% Methacrylic acid MAGIC gels: R 2 (1/s) versus dose (Gy) at 85 MHz [5]

4.6 Tissue Equivalency

Deene et al have reported polymer gels to be tissue-equivalent. Polymer gels, MAGIC gels, Fricke gels have electron densities within 1% of the electron density of the soft tissue and their effective atomic numbers are 7.4. The percentage amounts of the elements nitrogen, carbon, hydrogen, and oxygen in the MAGIC gels are very close to those in the soft tissue. The electron density and mean atomic number of the MAGIC gel are closer to those for muscle than for water [4].

Table 5.1 Comparison of elemental composition, electron densities and average atomic numbers for MAGIC gel, human muscle tissue and water [45]

Material	w_C	w_H	w_N	w_O	w_S	$w_{Cu(ii)}$	ρ (kg m^{-3})	ρ_e ($\times 10^{29}$ m^{-3})	ρ_e/ρ ($\times 10^{26}$ kg^{-1})	Z^a
MAGIC	0.0751	0.1062	0.0139	0.8021	2.58×10^{-6}	5.08×10^{-6}	1060	3.51	3.31	7.07
Muscle	0.1230	0.1020	0.0350	0.7298	0.00	0.00	1030	3.44	3.31	6.93
Water	0.00	0.1111	0.00	0.8889	0.00	0.00	1000	3.34	3.34	7.22

[a] Calculated as $Z = \Sigma_k w_k Z_k$.

4.7 MAGIC Gel Components

Copper sulphate (Cu_2SO_4* H_2O) and ascorbic acid form a complex with oxygen, which acts as a free radical to initiate polymerization of methacrylic acid. Hydroquinone prevents auto polymerization and absorbs any free radicals in the gel. The ascorbic acid is the oxygen scavenger. Copper sulphate acts as a catalyst in the oxidation of ascorbic acid[4].

According to Deene et al, when more hydroquinone is used, R2 is decreased showing an inhibitory effect. At higher concentrations, hydroquinone will scavenge both

oxygen and monomer radicals which will inhibit the polymerization reaction. In the presence of small amounts of ascorbic acid, less oxygen is scavenged by the copper–ascorbate complex and larger amounts of hydroquinone are needed to scavenge rest of the oxygen radicals [4, 44].

Fong *et al* showed that some initial polymerization occurs due to the creation of radicals from the ascorbate–copper–oxygen complex. At high $CuSO_4\ 5H_2O$ concentrations the polymerization reaction is terminated by a redox reaction [54].

In manufacturing process copper–ascorbate complex is formed. Oxygen reacts with this copper–ascorbate complex. As the result of electron transfer in the complex, the complex becomes a double radical product. This structure is unstable and will spontaneously release the copper ion with the formation of an ascorbate anion radical and a hydroxyperoxide radical. Eventually the copper ion is released and the ascorbate anion is further oxidized to dehydroascorbic acid. In the presence of monomers such as methacrylic acid, the radicals formed in final step will initiate a polymerization reaction. The formation of the complex-derived radicals may be summarized by the equations [44]:

$$AscA + O_2 + Cu^{2+} \rightarrow AscA - O_2 - Cu - Complex \quad (1)$$

$$AscA - O_2 - Cu - Complex \xrightarrow{kd} R_c^{\cdot} + Cu^{2+} \quad (2)$$

As radiation is incident on water in the polymer gels, free radicals, ions and other molecules are created. The free radicals launch the chain polymerization by creating radicalized free monomers. Afterwards oligomers and polymer radicals continue to propagate and finally polymerization terminates. In the normoxic gels, the ascorbic acid–metal complex with oxygen generates free radicals, which initiate polymerization. The gels are stable normally they do not significantly with the copper complex alone since without free radicals The radicals will initiate a polymerization and propagate in the same manner [4].

4.8 Dose Response Characteristics

In the dose range of 0-30 Gy, the dose–R2 curves are approximately linear and can be expressed as:

$$R_2 = R_0 + a\,D \qquad (3)$$

where R_0 is the relaxation rate of an unirradiated gel and a is the slope displaying the change of R_2 in unit dose [5].

The amount of methacrylic acid in the formulation has different effects on the gel. When we increase the amount of Methacrylic acid in the gel, the slope of the dose response curve increases. However, intercept of the response curve, which shows the R_2 of the unirradiated gel, also increases. Most probably this effect is due to the initial polymerization caused by remaining free radicals and amount of the acrylic monomers [5].

Methacrylic acid and hydroquinone are less toxic than acrylamide, being another advantage of MAGIC gels. Like the other polymer gels, MAGIC gels can take any shape of a container and make up an anthropomorphic phantom because of their tissue equivalence. The dose response is convenient for MRI and the dose range is comparable to the other gels. They are easier to manufacture, store and use [4]. New types of normoxic gels have been formulated as MAGAS and PAGAS. The acronym ‘MAGAS’ stands for Methacrylic Acid Gelatin gel with Ascorbic Acid as an anti-oxidant. The acronym ‘PAGAS’ stands for Poly-Acrylamide Gelatin gel with Ascorbic acid as an anti-oxidant [4].

4.9 Reactions in Normoxic Polymer Gels

When high energy photons pass through the polymer gel, they create a sparse track of ionization (Figure 4.4). The secondary electrons have sufficient energy to cause additional ionization events, which create many low-energy electrons. The radiochemical products are created in "spurs" which are clusters of ionization and excitations. The first products diffuse and react with other molecules. The first products occur in the pre-thermal phase, which is the first 10^{-14} to 10^{-15} seconds of the interaction. A local thermal equilibrium is established in the 10^{-12} seconds. After 10^{-8} seconds the intermediate products from the radiolysis of water are the aquatic electron, hydroxial ion (OH^-) and the hydroxium ion (H_3O^+). These products react with the monomers [57].

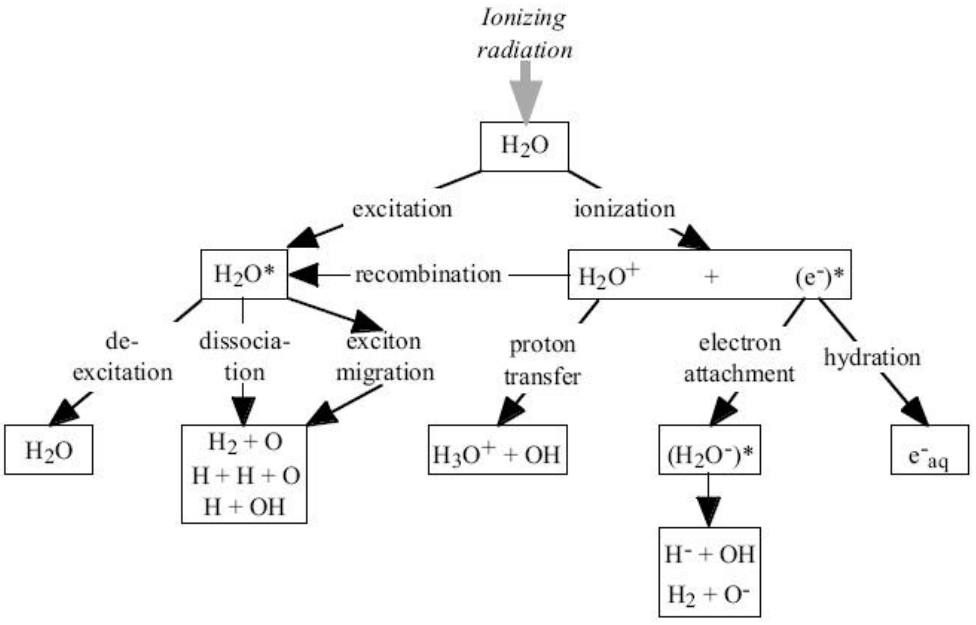

Figure 4.4: The typical reactions in the result of the radiation in water[57]

"In polymer gels, the polymerization is initiated by radical products created in the result of radiolysis of water, which can be represented as:

$$H_2O \xrightarrow{k_D} 2R^{\cdot} \qquad (4)$$

where k_D is the decomposition rate of water and R represents the radical.

Monomer radicals are formed when the radicals react with the monomers. Radicals represented as R react with monomer, as M, or with polymer, M_n *(where* $n > 1$) consisting of *n* monomer units, resulting monomer or polymer radicals, $RM_n^{\cdot}$

$$R^{\cdot} + M_n \xrightarrow{kI} RM_n^{\cdot} \quad \text{with } 1 \le n \le u \tag{5}$$

$k_I(n)$ is the initiation rate of a polymer with *n* monomer units and ? is the maximum chain length.

The electrons bind to the double bonds of the monomers and trigger the polymerization. The cross linking monomers have two double bonds which can be reactive in polymerization. The reaction rate decreases as the molecular size of the polymer increases. The shape and the location of double bonds are also factors in the polymerization rate [4].

The polymer radicals RM •react with other monomers or polymers M that results in larger polymer radicals:

$$RM_n^{\cdot} + M_m \xrightarrow{kp(n,m)} RM_{n+m} \tag{6}$$

k_P, the rate of propagation, is determined by the size and shape of the reacting particles. Different radicals may react with each other and terminate the chain polymerization. These reactions can be represented as:

$$R^{\cdot} + R^{\cdot} \xrightarrow{KT1} RR = I \tag{7}$$

$$R^{\cdot} + RM_n \xrightarrow{kT2(n)} I + M_n \text{ with } 1 \le u \tag{8}$$

$$RM_n^{\cdot} + RM_m^{\cdot} \xrightarrow{kT3(n,m)} I + M_{n+m} \qquad (1 \le n \le m \le u) \text{ and } (n + m \le u) \tag{9}$$

where I is a stable molecule.

The radical monomers can react with each other through redox reactions as:

$$RM^{\cdot}_{n} + RM^{\cdot}_{n} \xrightarrow{kT4(n,m)} I + M_{n} + M_{m} \qquad (1 \le n \le m \le u) \text{ and } (n + m \le u) \qquad (10)$$

When oxygen is present, peroxides are created that stop the growth of polymer chains "[4].

4.10 Macroscopic Effects of Ionizing Radiation in Gels

"According to Deene, the protons in a polymer gel can be grouped into three ensembles:

a) Protons from the free water molecules and monomers
b) Protons from the growing polymer and protons of water bound to macromolecules
c) Protons from the gelatin matrix and water molecules bound to gel

The spin-spin relaxation is the result of loss in the phase coherence due to the micro-magnetic variances and coupling of the neighboring protons.

We define the spin-spin relaxation rates of these proton pools as $R_{2\ mob}$, $R_{2\ poly}$, R_{2gela} respectively. If the lifetimes of protons in these environments are short compared to the correlation times; the total relaxation curve is mono-exponential with a relaxation rate that is the equal to the weighted average of the relaxation rates of these proton pools:

$$R_2 = f_{mob} * R_{2\ mob} + f_{poly} * R_{2\ poly} + f_{gela} * R_{2\ gela} \qquad (11)$$

Before the irradiation, the second pool is empty while the first pool is at its maximum. When irradiated, the second pool increases while the first proton pool

decreases on behalf. As a result, the relaxation rate changes with the amount of polymerization.

The mobility of the molecules, the exchange rates of the protons and the pH of the gel determines the relaxation rates of different proton pools" [44].

4.11 Calibration of the Dosimeter

The environmental and physical conditions during manufacturing and the purity of chemicals affect the sensitivity and the response of the particular polymer gel. Thus each gel sample should be calibrated on its own [44]. Different methods for dosimeter calibration have been studied. In these methods, gel samples are irradiated at predefined dose levels. The scanned MRI images of the calibration gel samples create a dose curve against the obtained relaxation rates R_2 ($=1/T_2$). This curve is the reference curve used to calibrate the phantoms in radiation scenarios [54, 58].

In the multi flask method, several small containers are filled with gel and every single container is irradiated to a predefined dose with a 180^0 opposite beam positions to create a uniform dose distribution throughout the gel sample [54]. The dose-R_2 curve is reported to be linear in the range of 0-30 Gy for the MAGIC gel [46].

5. GEL PREPARATION

5.1 Introduction

The gel mixture was manufactured under the normal atmospheric conditions as in the formulation proposed by Fong et al [5]. The gel is composed of 8% gelatin by weight (300 bloom Sigma; St Louis, MO), 9% methacrylic acid by weight (Sigma; St Louis, MO), ascorbic acid (2 mmol/l), $CuSO_4$*5 H_2O (0,02 mmol/l), hydroquinone (1 mmol/l) and de-ionized water [Table 6.1].

To manufacture the normoxic polymer gel, the following items are used: an electronic balance (10 mg scale), a mercury thermometer, different glass flasks, beakers, vessels, a heater and a magnetic stirrer. The mixture was prepared in a fume cupboard. The solutions were heated, with a thermostatically controlled electrical heating plate equipped with magnetic stirring.

To obtain 4,5 liters of gel, the following procedure was followed: 3235,5 ml of de-ionized water and 360 g of gelatin were placed in a beaker, the gel powder was left in water for 15 minutes, at room temperature until it was totally dissolved. Later, the beaker was heated in the electrical oven to 45 °C, and then was taken out and placed on the electrical heating plate with magnetic stirring until it was heated up to 50 °C and a clear solution was obtained. When the gelatin has completely melted and become almost homogeneous, the beaker was allowed to cool down to 35 °C. In the meantime, three different solutions were produced: 4,40 g of hydroquinone diluted in 400 ml of de- ionized water, 0,25 of copper sulphate diluted in 100 g of water and 1,76 g of ascorbic acid diluted in 100 g of water. Then 100 g of the ascorbic acid solution and 4,5 g of copper sulphate solution were poured into the hydroquinone solution and mixed together. The hydroquinone-copper sulphate and ascorbic acid mixture together with 360 g of methacrylic acid were added to the cooled gelatin solution while stirring it continuously.

Finally the anti-oxidant was added to minimize any additional oxygen penetrating through the gel. The solution was stirred until the mixture is homogeneously dissolved.

Methacrylic acid is the monomer. Ascorbic acid together with copper sulphate build complexes, which will act as oxygen scavenger and will bind to the oxygen dissolved in the gel.

Table 5.1- Chemical Formula of the MAGIC Gel [60]

Component	**Concentration**
Gelatin Type A from porcine skin Sigma Bloom 300	8%
Hydroquinone, 99%	10mmol/l
Ascorbic Acid, 99%	2 mmol/l
$CuSO_4$*5 H_2O	0,02 mmol/l
Methacrylic acid	9%
Distilled water	83%

The gel was poured into two 2-liter capacity spherical glass balloons and into six 100-ml volume PVC vials (Figure 5.1). The balloon had a diameter of 16 cm; for the inhomogeneous phantom and a cork was placed to represent the air cavity. Stereotactic frames and fiducial markers were attached to the phantoms for MR scanning and image processing. The vials were used in order to obtain the dose-R2 calibration curve. The balloons and vials were protected of the UV radiation from sunlight by wrapping them with aluminum foils. The gels at room temperature, were kept in the dark for approximately 10 hours until total solidification occurred and then kept in the refrigerator. For other polymer gel systems, a minimum time of 10 hours (PAG) and 30 hours (MAGIC

gel) is recommended between irradiation of the samples and the MR scanning, to allow the termination of polymerization. In this study, MR images were acquired approximately 30 hours following the irradiation.

5.3 Gel Irradiation

The gel samples were allowed to stabilize to room temperature, before the irradiation. For irradiation of the vials, Cobalt 60 teletherapy (Theratron 780 C, Theratronics, Canada) unit was used. Each vial was placed such that the center of the vial was in the central axis of a 30 cm x30 cm x30 cm water tank, at a depth of 10 cm from the surface. The central point of the vial had a Source to skin distance (SSD) of 80 cm and was irradiated with a field size of 10cm x 10 cm. The vials were irradiated by 50% of the dose from the front and by 50% of the dose from the rear, by turning the gantry by 90^{0} and 270^{0} respectively to generate a uniform dose distribution throughout the vial. The vials were then exposed to doses of 3, 5, 7, 10, 15 and 20 Grays.

Figure 5.1: The calibration vials

In the paranosal sinuses cavity measurement, for the inhomogeneous phantom, a tumor near the paranosal sinuses cavity was simulated at a distance of 4 mm from edge of the cork. The simulated tumor was given one shot of radiation with a dose of 20 Gray in the Gamma Knife, using the 18 mm Helmet (figure 5.2 and 5.3).

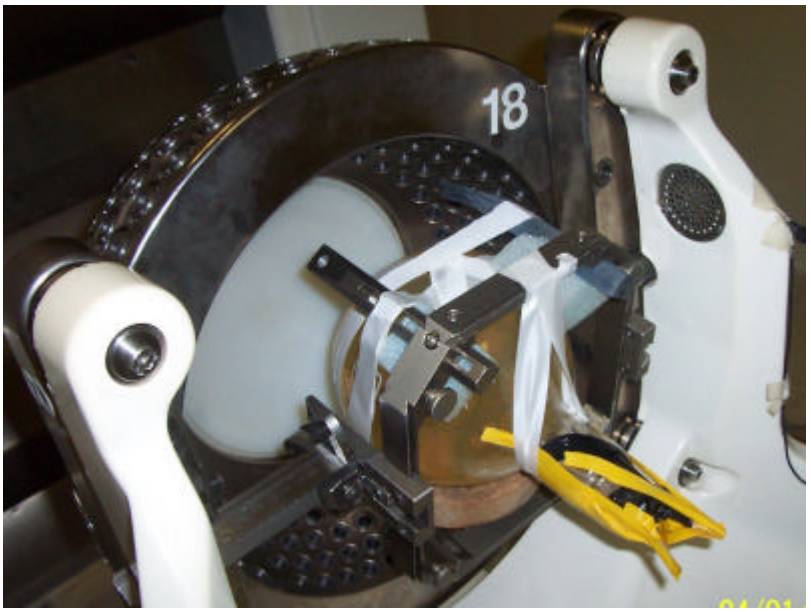

Figure 5.2: Irradiation of the inhomogeneous phantom in the Gamma Knife

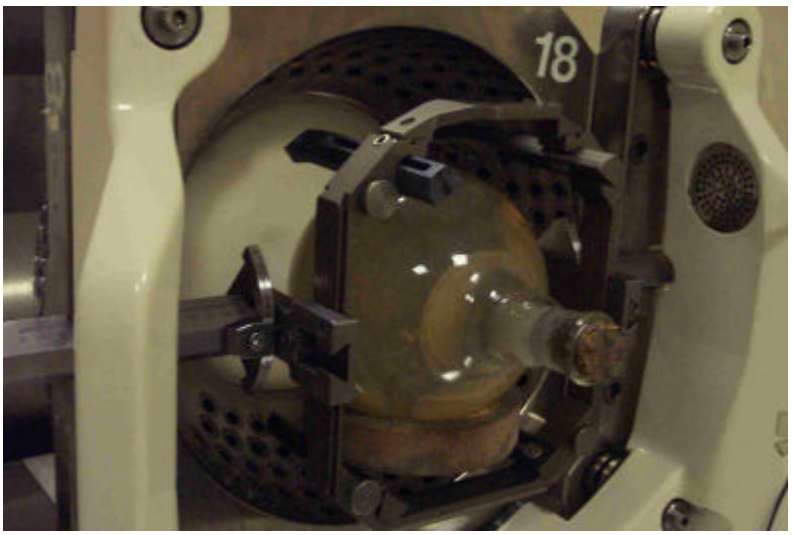

Figure 5.3: Irradiation of the homogeneous phantom in the Gamma Knife

In the auditory canal cavity measurement, for the inhomogeneous phantom, an acoustic neuroma was simulated at 4 mm from the edge of the cork. The simulated tumor was also given a shot of radiation at a dose level of 20 Gray in the Gamma Knife using again the 18 mm Helmet.

The treatment plans were performed in the GammaPlan using the MR images obtained before the irradiation. The homogeneous phantoms were irradiated with the same dose at identical coordinates as the inhomogeneous phantom (Figure 5.2 and 5.3). The balloons were placed identically in the Stereotactic frames by using lasers of the radiotherapy simulator (Figure 5.4). The stereotactic frame was placed horizontally and leveled with a water balance. The middle line of the phantom was marked from the two sides, by the side lasers and in the mid point on the top by the sagittal laser of the simulator. Hence the centers of the two phantoms were placed at the same point in the stereotactic frames. This way one can make a comparison between the physical dose distributions in the inhomogeneous and homogeneous phantoms.

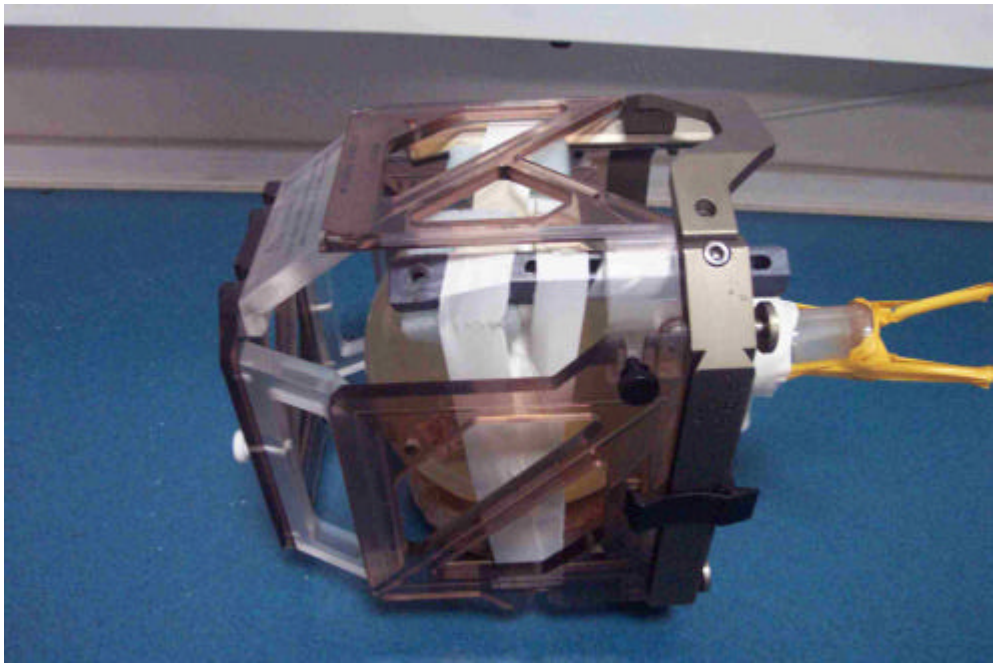

Figure 6.2: The irradiated inhomogeneous phantom attached with the stereotactic frame for MR Imaging.

5.4 Phantom Evaluation

The phantoms and vials were scanned in a 1.5 Tesla MR Unit using the head coil for signal reception. The transverse relaxation rate R_2 of the water protons was chosen as a measure of the absorbed radiation. Gel samples were left in the MR room 24 hours before the scanning operation, to obtain temperature equilibrium throughout the gel. For the calculation of the dose distributions in the phantoms, T2 mapping of the irradiated normoxic gel is computed using the slice selective Spin Echo MR sequence.

In the auditory canal cavity experiment, the RF sequence with TR=2000 ms and TE=10, 100, 110, 120, 170 and 269 ms were selected for the phantoms and the vials. The homogeneous and inhomogeneous phantoms were scanned at 9 slices of width 3 mm. Inter echo time was 10 ms, the field of view was 300 mm with a matrix size of 256×256. The temperature was measured before and after each measurement using a standard alcohol thermometer. The average temperature was 22 ^{0}C and it remained stable within 1 ^{0}C.

To obtain the true T_2 values, images were obtained from the axial mid-plane for the calibration vials.

In the paranosal sinuses cavity experiment, the RF sequence was adjusted to TR=3000 ms and TE=10, 50, 100, 150 and 200 ms for the phantoms. The homogeneous and inhomogeneous phantoms were scanned with a slice width 3 mm. Inter echo time was 12 ms, the field of view 300 mm with a matrix size of 256×256. Again, the temperature was measured to be stable within 1 ^{0}C. The vials were scanned in an MR sequence with TR=3000 ms and TE ranging from 15 ms to 495 ms, increased in steps of 15 ms.

6. RESULTS

MR images of the phantoms recorded in a compact disc are transferred to a personal computer. A specially written software in MATLAB is run to calculate the pixel-by-pixel true T_2 values of the images of each slice. The R_2 relaxation rate of the pixel was computed by fitting the signal intensity for each echo time to a mono-exponential decay, using a non linear minimization algorithm based on the Levenberg–Marquardt method. T_2 images were then reconstructed using the T_2 relaxation time constants (Figure 6.1). The single exponential equation can be expressed as:

$$I(t) = M_0 \exp(-TE/T_2) \quad (1)$$

Where, M_0 is the proton density, TE is the echo time and T_2 is the transverse relaxation time constant.

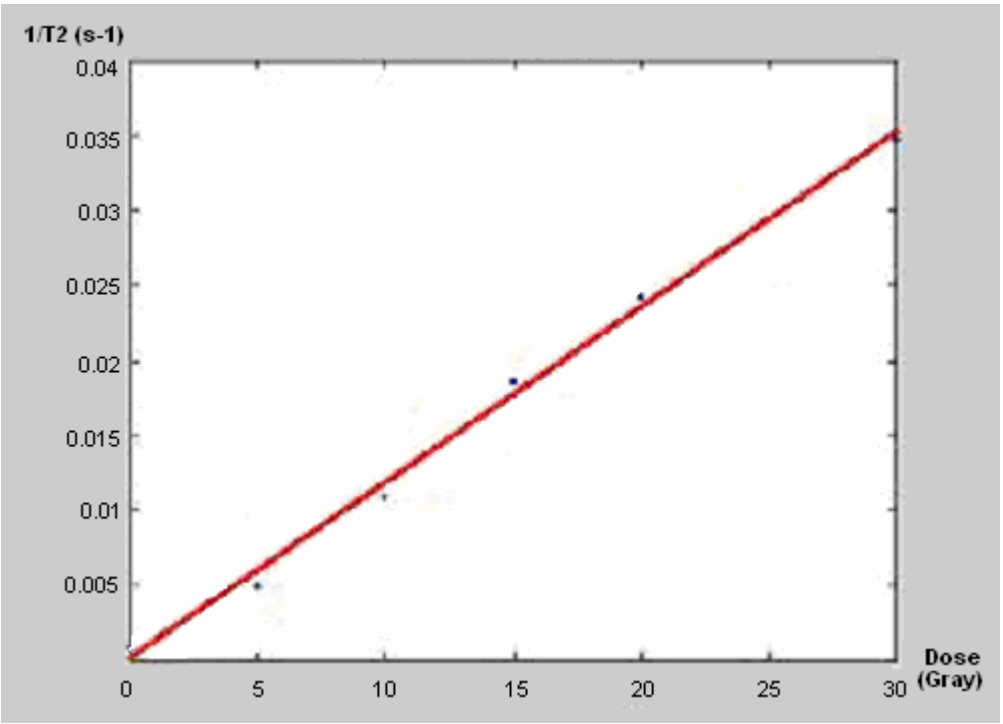

Figure 6.1: The Calibration curve in the auditory canal cavity experiment: R2 (sec^{-1}) vs. Dose (Gy). (the regression coefficient =0,99) from the Cobalt Therapy machine

The calibration curve is derived by the multiple flask method. The calibration curve, which is linear in the range from 0 to 20 Gy is then used to convert the R_2 values of each pixel to the corresponding dose value (Figure 6.1).

In the calculated dose mappings of the phantoms, a rectilinear coordinate system is positioned at the center of the shot. In the axial plane of view, the horizontal axis is parallel to the X-axis and the vertical plane is parallel to the Y-axis of the Stereotactic frame. In the coronal plane view, the horizontal axis is parallel to the X-axis and the vertical axis is parallel to the Z-axis of the stereotactic coordinate system. In the saggital view, the horizontal axis is parallel to the Z-axis and the vertical axis is parallel to the Y-axis of the Stereotactic coordinate system.

The dose profiles are computed and drawn in the horizontal and vertical axes of this coordinate system. As seen from the dose profiles in Figures 7.10 and 7.11, the points of intersection of the 30%, 50% and 70% isodose lines with the coordinate system are determined. The distances between the intersection points of the isodose curves with the coordinate axes, in the opposite sides of the origin, give the diameters in the vertical and the horizontal axes. The GammaPlan dose distributions in both phantoms are compared among themselves and with the gel dosimetry dose mappings, using the vertical and horizontal diameter of the 30%, 50% and 70% isodose curves (Table 6.6 and 6.7).

6.1 Simulation of the Auditory Canal Cavity

Dose distributions near the dose maximum point, along the three axes of the homogeneous and in homogeneous phantoms, are calculated and mapped. The GammaPlan predicted dose distributions (Figure 6.2 and 6.3) are compared with the gel dosimetry results. Dose distributions were compared in the slices where the maximum dose has the largest area. In Leksell frame coordinates, this slice was located at Z= 105 in the axial plane and at Y= 105 in the coronal plane.

By using the fudicial markers and Leksell frame coordinates; identical slices were determined as in the GammaPlan images. The 30%, 50% and the 70% isodose diameters in the GammaPlan slices were measured using the pointer system on the GammaPlan monitor.

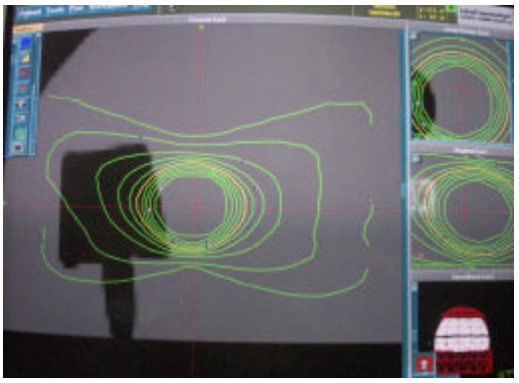

Figure 6.2: The GammaPlan for the inhomogeneous phantom in the auditory canal cavity experiment

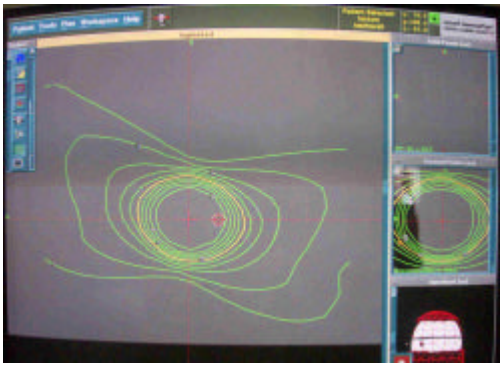

Figure 6.3: The GammaPlan for the homogeneous phantom in the air cavity experiment

As seen in Table 6.3, the diameters of the isodose curves obtained with gel dosimetry in the homogeneous phantom are very close to those predicted by the GammaPlan, for the same phantom. From the dose mappings of GammaPlan and gel dosimetry, it is clearly seen that the dose distribution in the homogeneous phantom calculated by the gel dosimetry is in good agreement with the GammaPlan calculated dose

distribution. This verifies that the gel dosimetry can be a very useful tool in calculating the relative dose distributions in Gamma Knife treatment.

However, as seen in Table 6.4 and Figures 6.5, 6.6, 6.7, 6.8, 6.9 and 6.10, the dose distribution in the inhomogeneous phantom exhibits significant differences from that of the homogeneous phantom. The dose distribution in the inhomogeneous phantom shows dose decrease near the inhomogeneity and perturbation by the air cavity. The 30%, 50% and 70% isodose curves in the inhomogeneous phantom dose mappings are all asymmetric with respect to the shot center due to the effects of the air cavity. As seen in the figure 6.8, 6.10 and 6.12 for the inhomogeneous phantom, the vicinity of the cork shows much less accumulated dose compared to the GammaPlan predicted dose distribution.

Figure 6.4: The irradiated homogeneous phantom

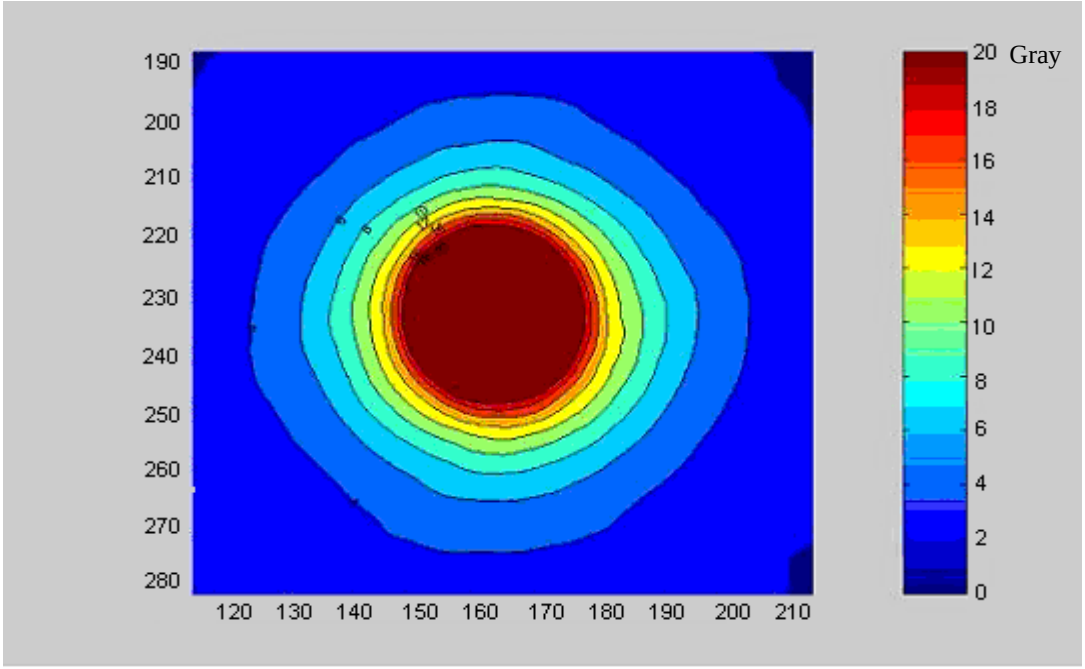

Figure 6.5: Homogeneous phantom dose distribution (Gy) in the axial plane, for slice Z=105 in stereotactic frame coordinates.

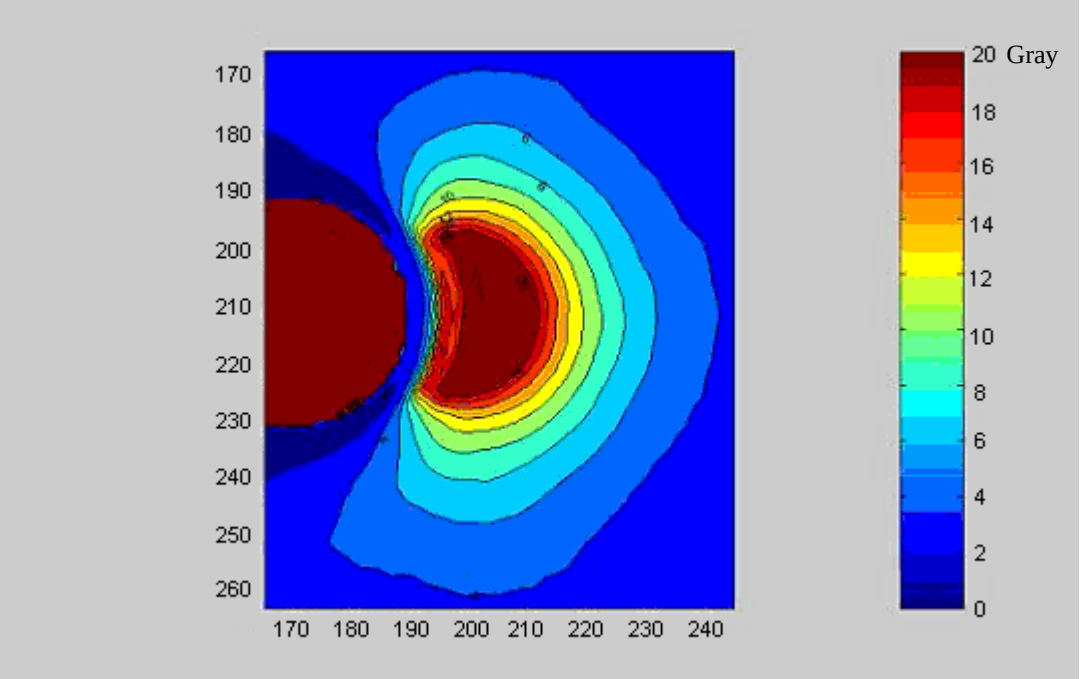

Figure 6.6: Inhomogeneous phantom dose distribution (Gy) in the axial plane, for slice Z=105 in stereotactic frame coordinates.

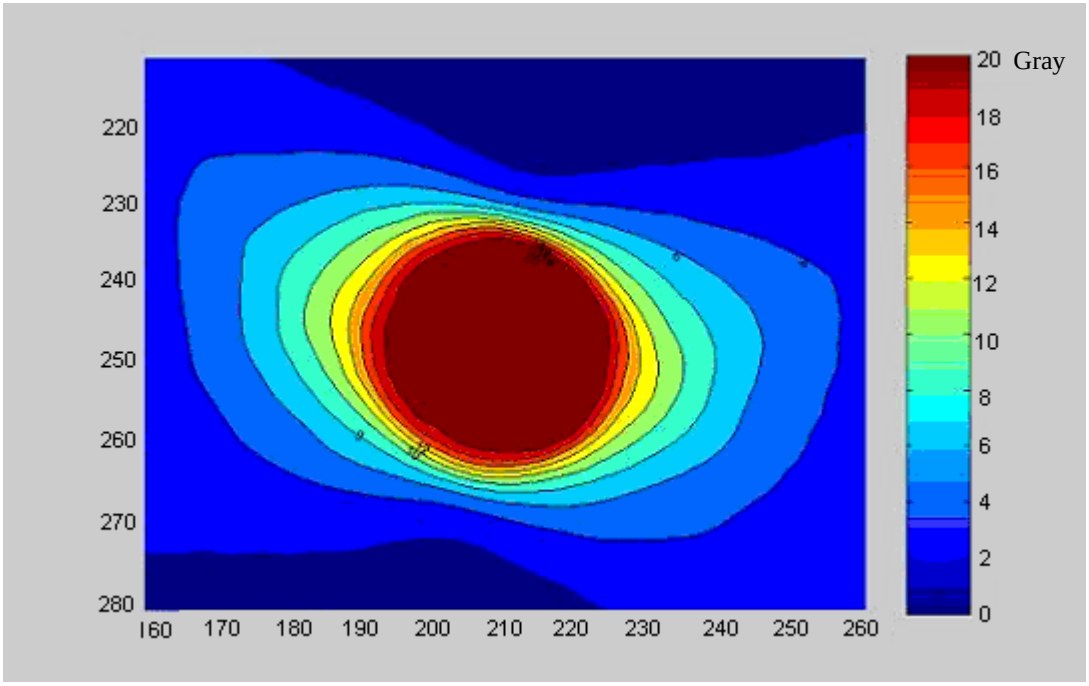

Figure 6.7: The isodoses in the homogeneous phantom dose distribution (Gy) in the coronal plane, for slice Y=105 in stereotactic frame coordinates.

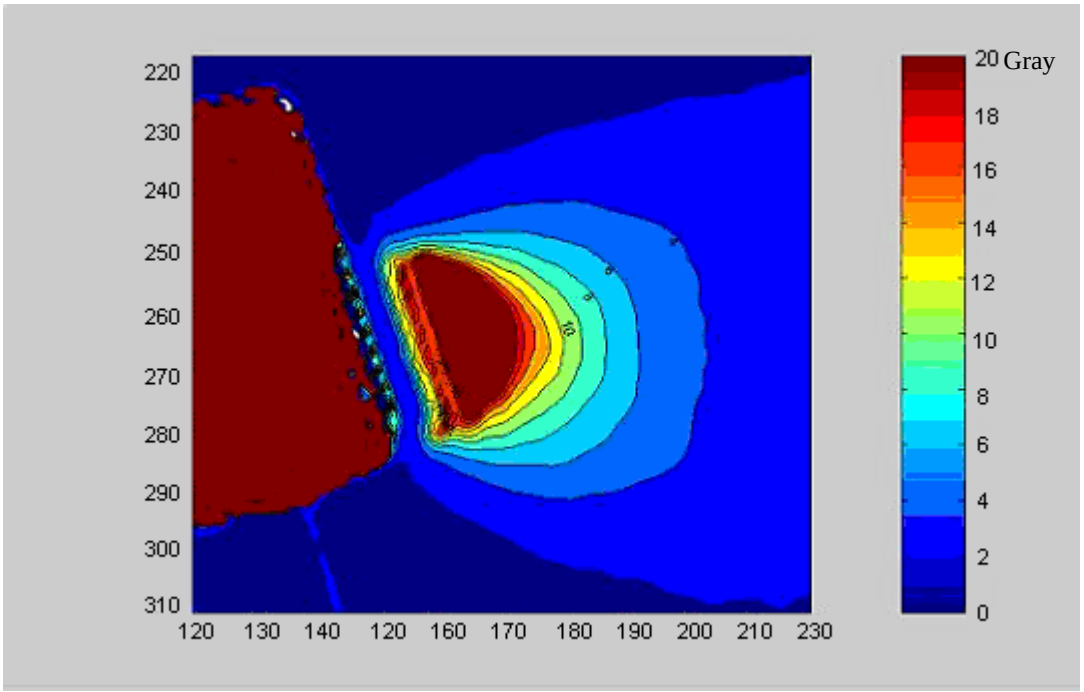

Figure 6.8: The isodoses in the inhomogeneous phantom dose distribution (Gy) in the coronal plane, for slice Y=105 in stereotactic frame coordinates.

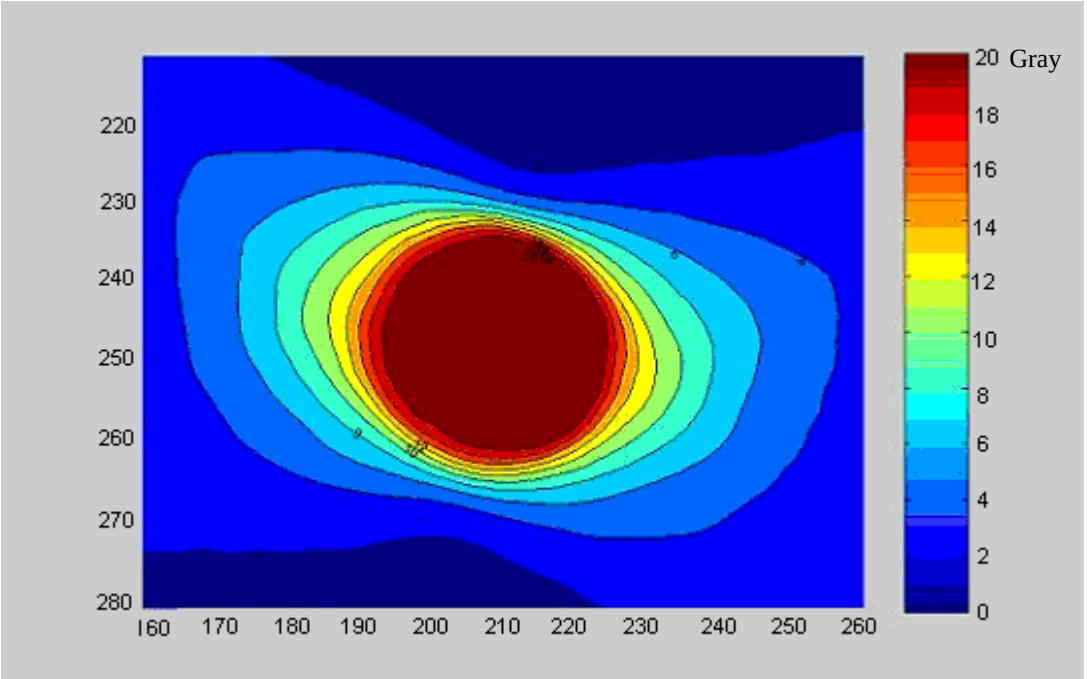

Figure 6.9: Homogeneous phantom dose distribution (Gy) in the Sagittal Plane, for slice X=63,5 in stereotactic frame coordinates.

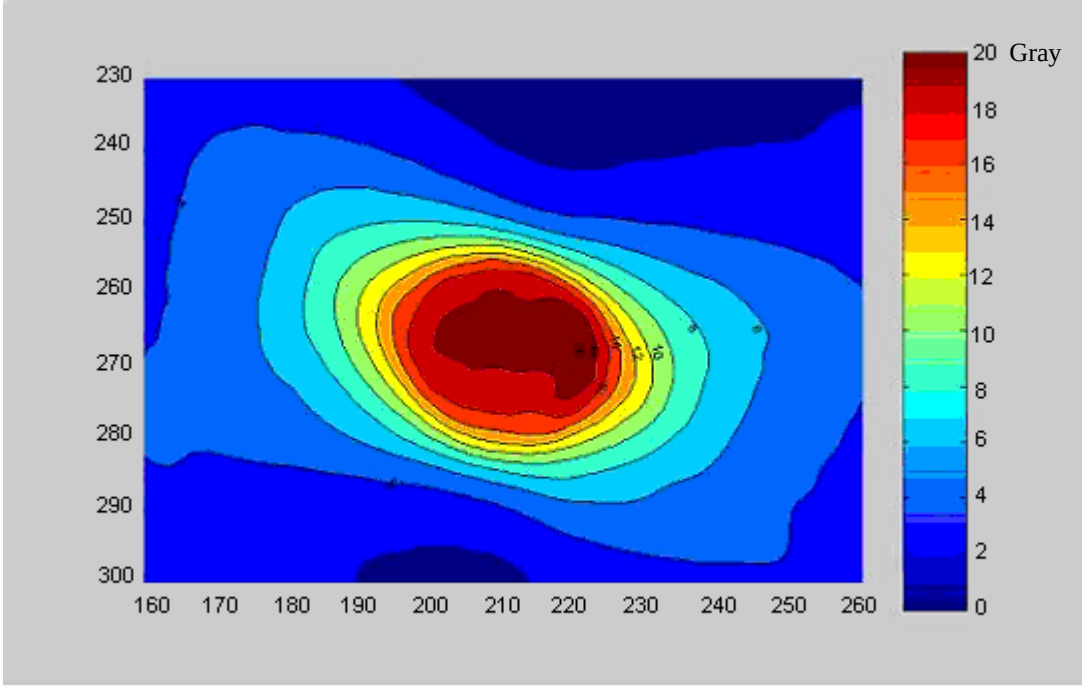

Figure 6.10: Inhomogeneous phantom dose distribution (Gy) in the Sagittal Plane, for slice X=63,5 in stereotactic frame coordinates.

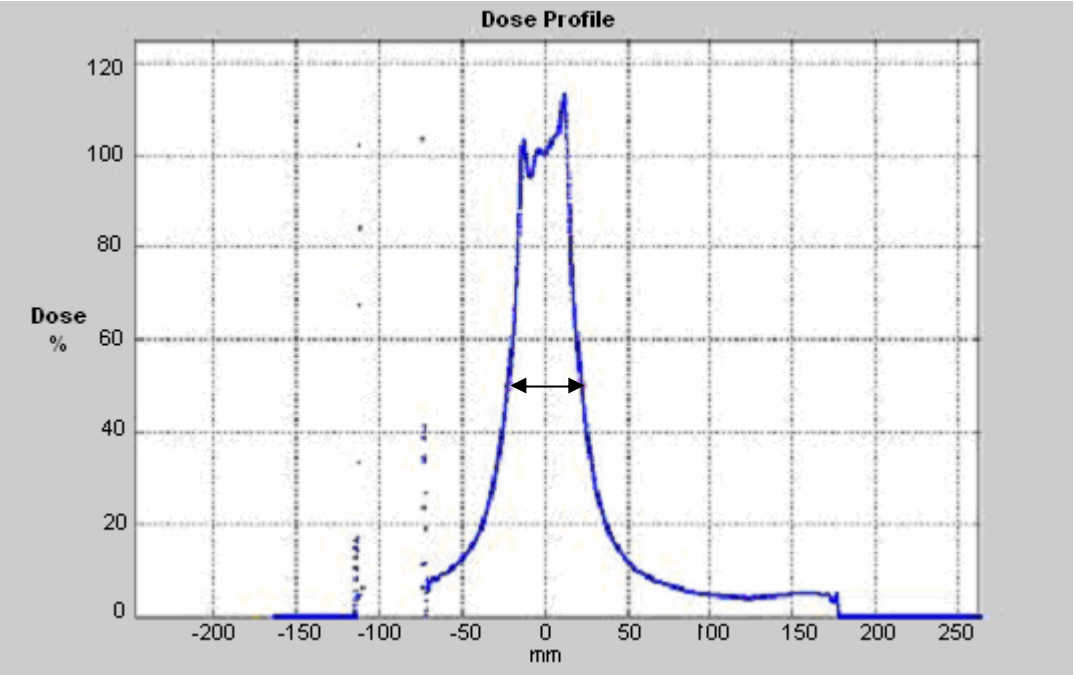

Figure 6.11: The dose profile on the X axis in the coronal Plane view for slice Y=105 (in terms of Leksell frame coordinates) for the homogeneous phantom of the auditory canal cavity experiment. The distance between the points corresponding to the 50 % on the dose profile curve gives the diameter of the 50% isodose curve.

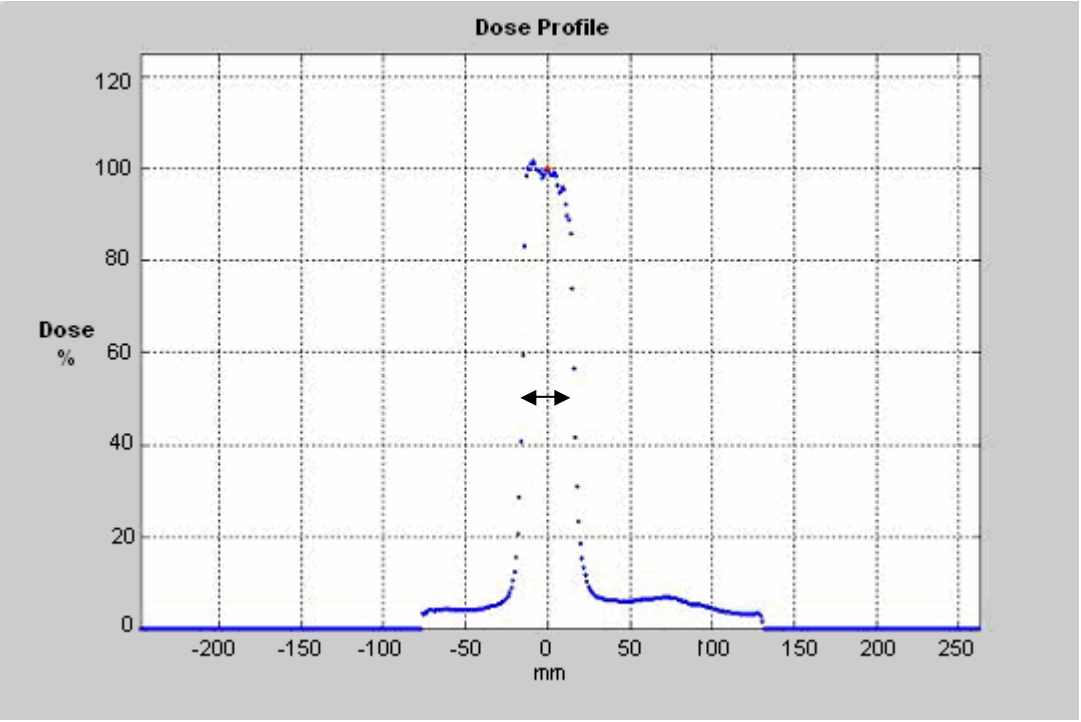

Figure 6.12: The dose profile along the Y axis in the coronal plane vie w for slice Y=105 (in terms of Leksell frame coordinates) for the homogeneous phantom of the auditory canal cavity experiment.

Table 6.3: Isodoses predicted by the GammaPlan

		Image Type	Leksell Frame Axis	70% Isodose (mm)	50% Isodose (mm)	30% Isodose (mm)
GammaPlan Predicted	Inhomogeneous Phantom	Axial [z=105 mm]	X	20	24,2	32,1
			Y	19,7	23,8	31,1
		Coronal [y=105 mm]	X	20,4	24,3	32,6
			Z	18,2	19,7	22,2
	Homogeneous Phantom	Axial [z=105 mm]	X	19,3	24,3	32,2
			Y	18,9	23,2	31,3
		Coronal [y=105 mm]	X	20,4	24	32,4
			Z	17,9	19,8	22,1

Table 6.4- Isodose measurements with the gel dosimetry

		Image	Leksell Frame Axis	70% Isodose (mm)	50% Isodose (mm)	30% Isodose (mm)
Gel Dosimetry Calculated	Inhomogeneous Phantom	Axial [z=105 mm]	X	12,4	15,8	21,5
			Y	19,5	25,2	38,3
		Coronal [y=105 mm]	X	10,3	15,6	21,7
			Z	15,9	17,6	20,6
	Homogeneous Phantom	Axial [z=105 mm]	X	19,3	24,3	34,2
			Y	19,4	23,6	31,6
		Coronal [y=105 mm]	X	20,1	25,8	34,7
			Z	17,4	18,5	20,3

6.2 Paranosal Sinuses Cavity Measurements:

In the paranosal sinuses cavity experiment, two spherical 2 liter capacity glass balloons were the phantom containers. Both glass balloons were filled with the MAGIC gel. The gel was prepared at the Chemistry Laboratory in Bogazici University. Seven plastic vials of 100 ml were filled with the gel and were irradiated with doses of 0, 3, 5, 10, 15, 20 and 25 Gy with the Cobalt-60 TeleTherapy machine (Theratron 780 C, Theratronics, Canada) respectively.

In this experiment, a lesion in the head near the paranosal sinuses is simulated. The inhomogeneous phantom was prepared by placing a cylindrical cork to represent the air cavity: the cork diameter was 2.5 cm and the length 8 cm. The homogeneous phantom simulates the physical structure considered in the GammaPlan.

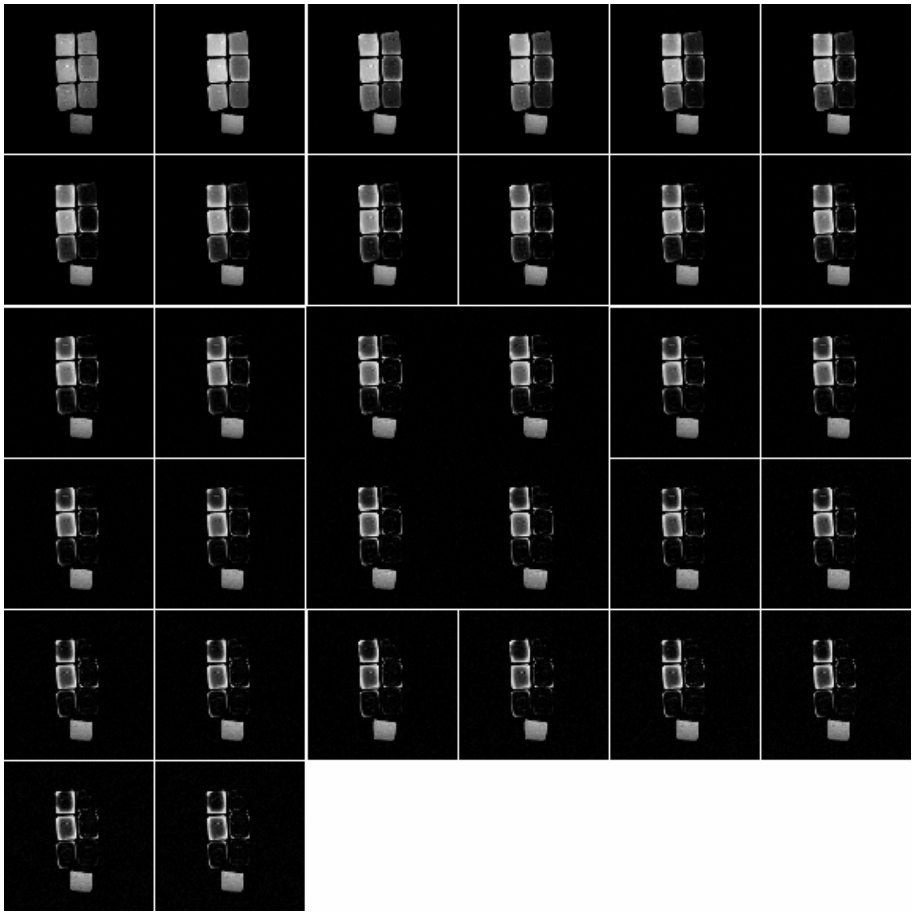

Figure 6.13: MR images of the vials filled with the gel, used for calibration.

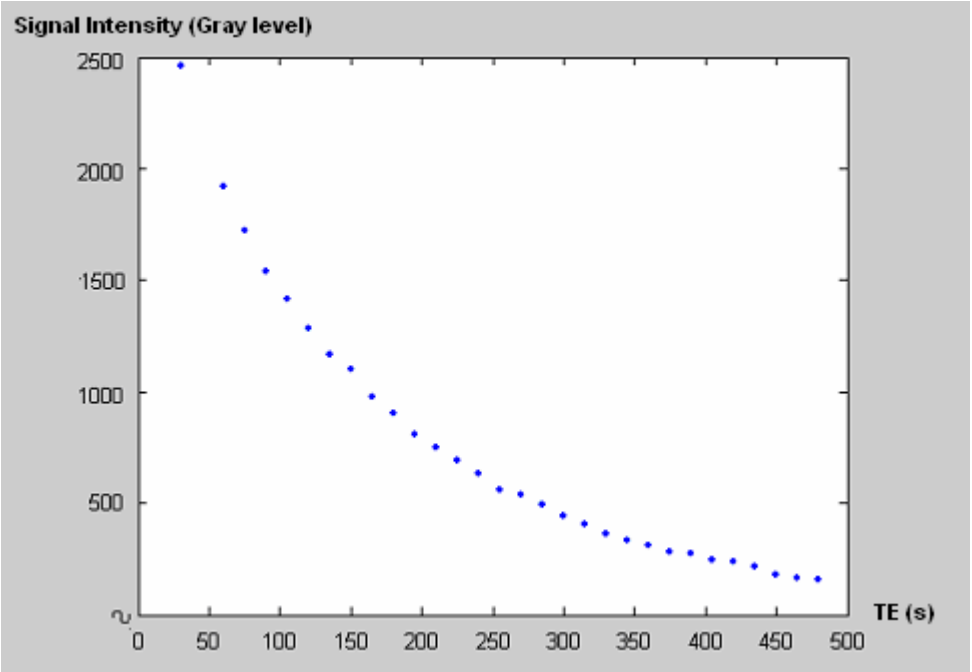

Figure 6.14: The exponential curve for the vial irradiated at 20 Gy where the vertical axis is the signal intensity and horizontal axis is the time to echo values. The vials were scanned in an MR sequence, with TR=3000 ms and TE increased from 15 ms to 495 ms, in steps of 15 ms.

In the inhomogeneous phantom, a shot of 20 Gy was given to a point at a distance of 4 mm. from the cork edge. The same amount of dose was applied at the same coordinates in the homogeneous phantom. The homogeneous and inhomogeneous phantoms were positioned spatially identical in the stereotactic frame using a radiotherapy simulator and lasers. The centers of both phantoms were positioned in the same stereotactic coordinates.

In the paranosal sinuses cavity simulation, the dose distributions in the axial axis slices with a slice distance 4 mm from each other are calculated and mapped in the homogeneous and inhomogeneous phantoms (Figure 6.11and Figure 6.12). The diameters of the 30%, 50% and the 70% isodose curves were calculated to compare the dose distributions proposed by the GammaPlan with those in gel dosimetry. Thereafter, the profiles obtained by the gel dosimetry for both phantoms are compared with the profiles obtained for the corresponding slices by the GammaPlan. The slices compared were those where the dose maximum areas were the largest. These were the slices Z= 71, 76 and 81

mm in the axial plane. By using the fudicial markers and Leksell frame coordinates identical slices were chosen in the GammaPlan images. The 30%, 50% and the 70% isodose distances in the GammaPlan slices were measured using the pointer system on the GammaPlan monitor.

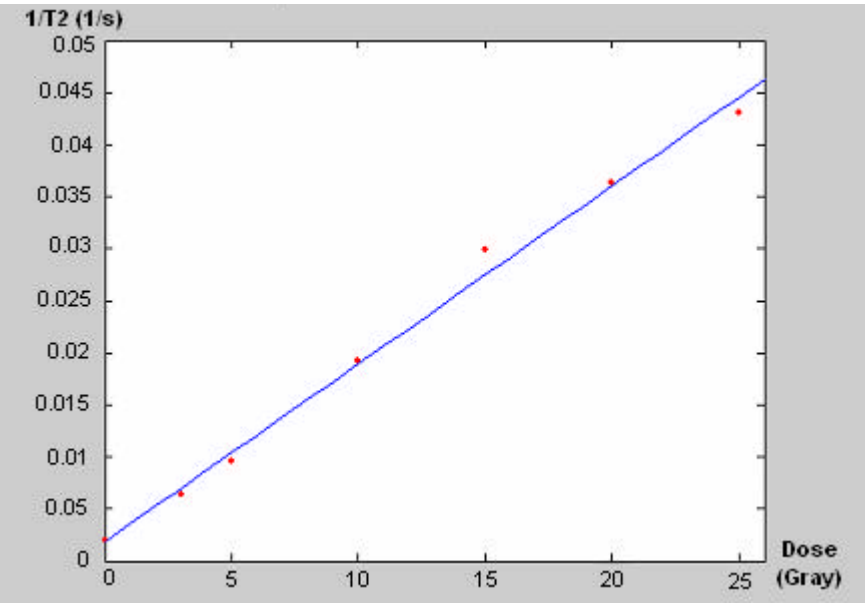

Figure 6.15: The calibration curve obtained by fitting the 1/T2 $(sec)^{-1}$ values to dose delivered to the vials irradiated in the Cobalt Therapy machine (regression coefficient =0,99).

In the homogeneous phantom, the dose distributions calculated by the gel dosimetry agree well with the GammaPlan calculated dose distribution. However, the dose distribution in the inhomogeneous phantom shows significant differences with that of the homogeneous phantom, representing the dose distribution proposed by the GammaPlan. The dose distribution in the inhomogeneous phantom shows perturbation by the air cavity

In the inhomogeneous phantom, the 30%, 50% and 70% isodose curves in the vertical axis are asymmetric with respect to the shot center due to the dose decrease caused by the air cavity. As seen in Figure 6.18, in the vicinity of the cork much less dose is accumulated compared to the GammaPlan predicted dose distribution.

Figure 6.16: The localization images of the inhomogeneous phantom, in the axial plane

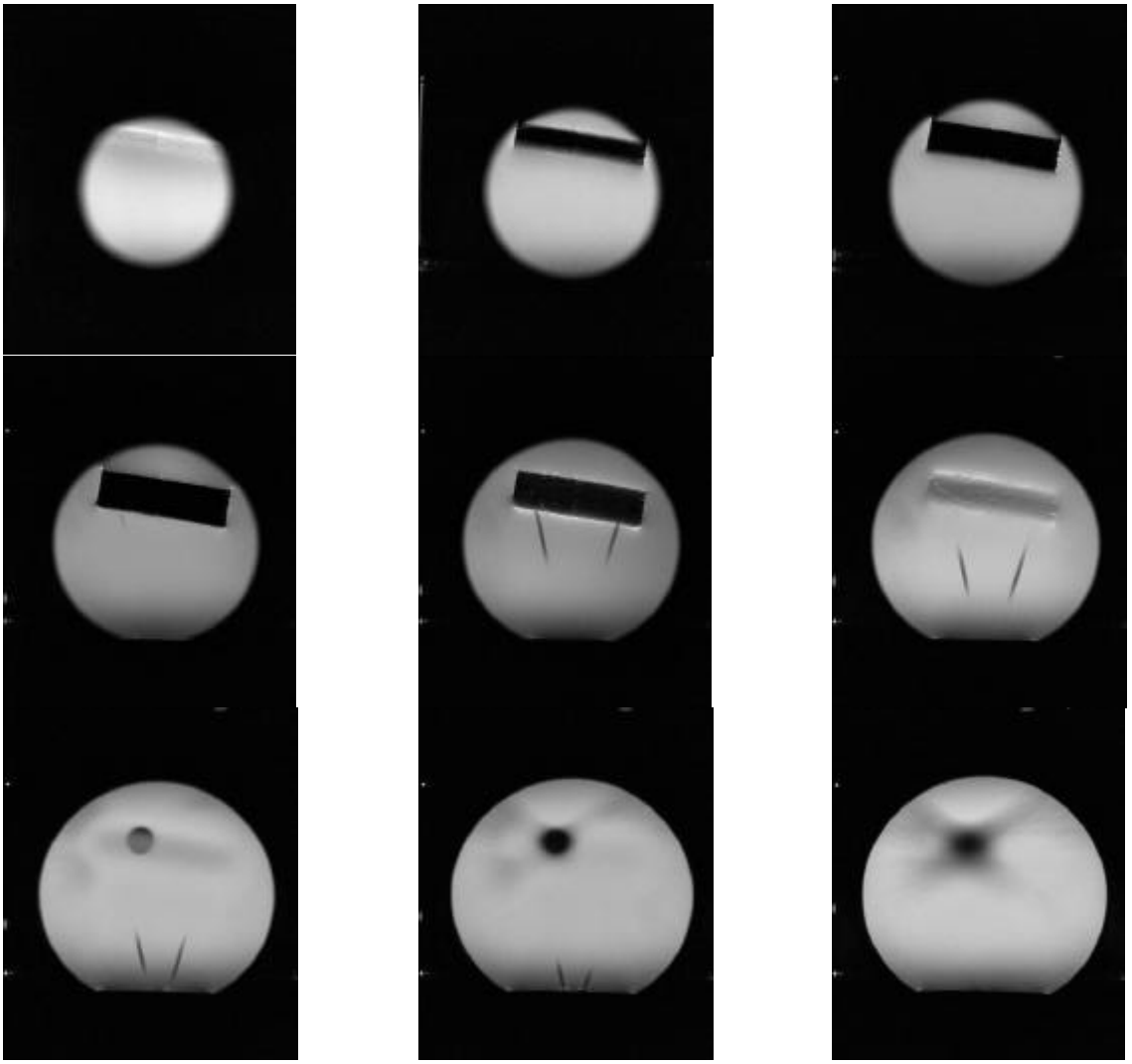

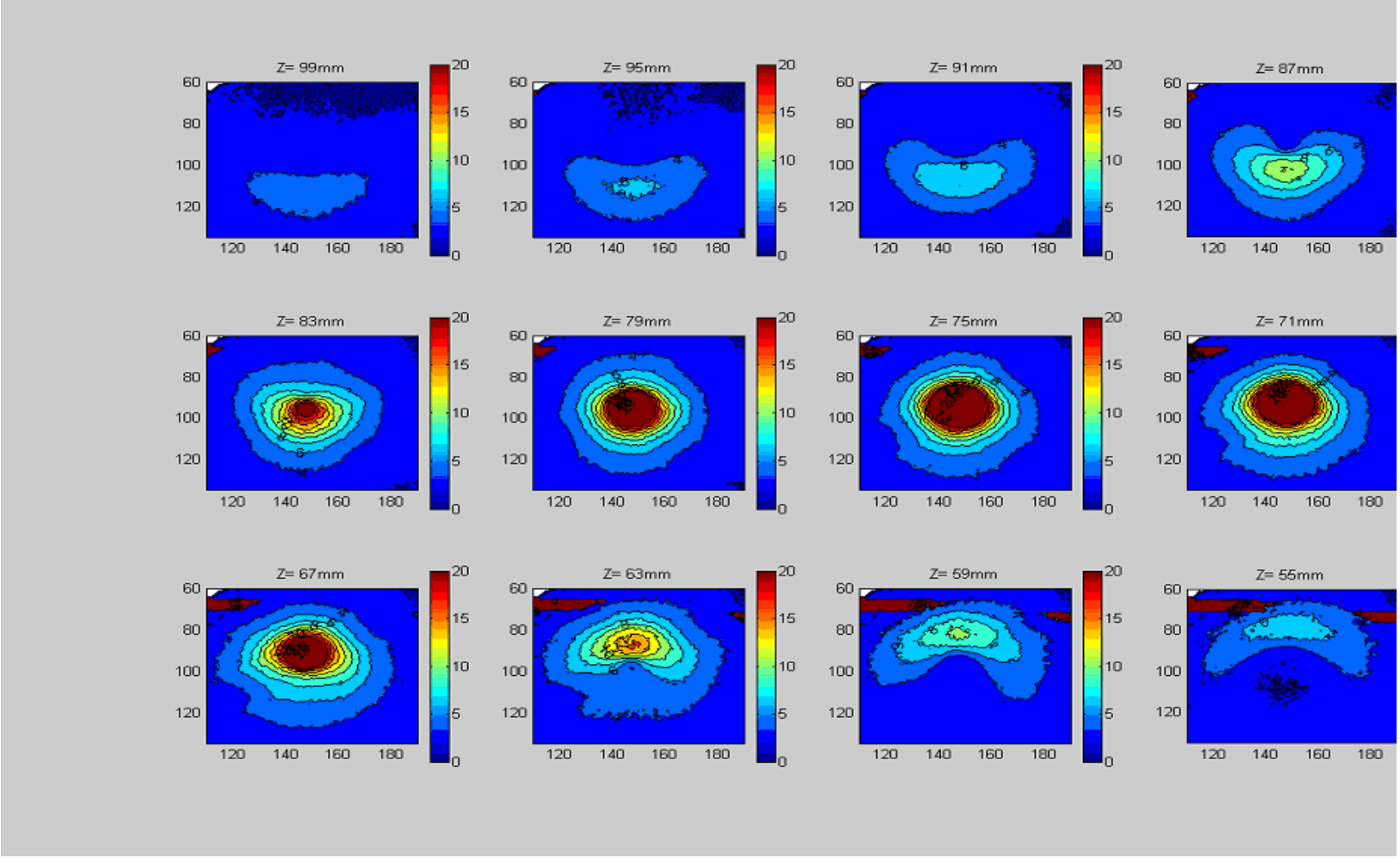

Figure 6.18: The dose mappings in slices of Z=55, 59, 63, 67, 71, 75, 79, 83, 87, 91, 95 and 99 mm in the axial plane of the homogeneous phantom, in the paranosal sinuses cavity experiment.

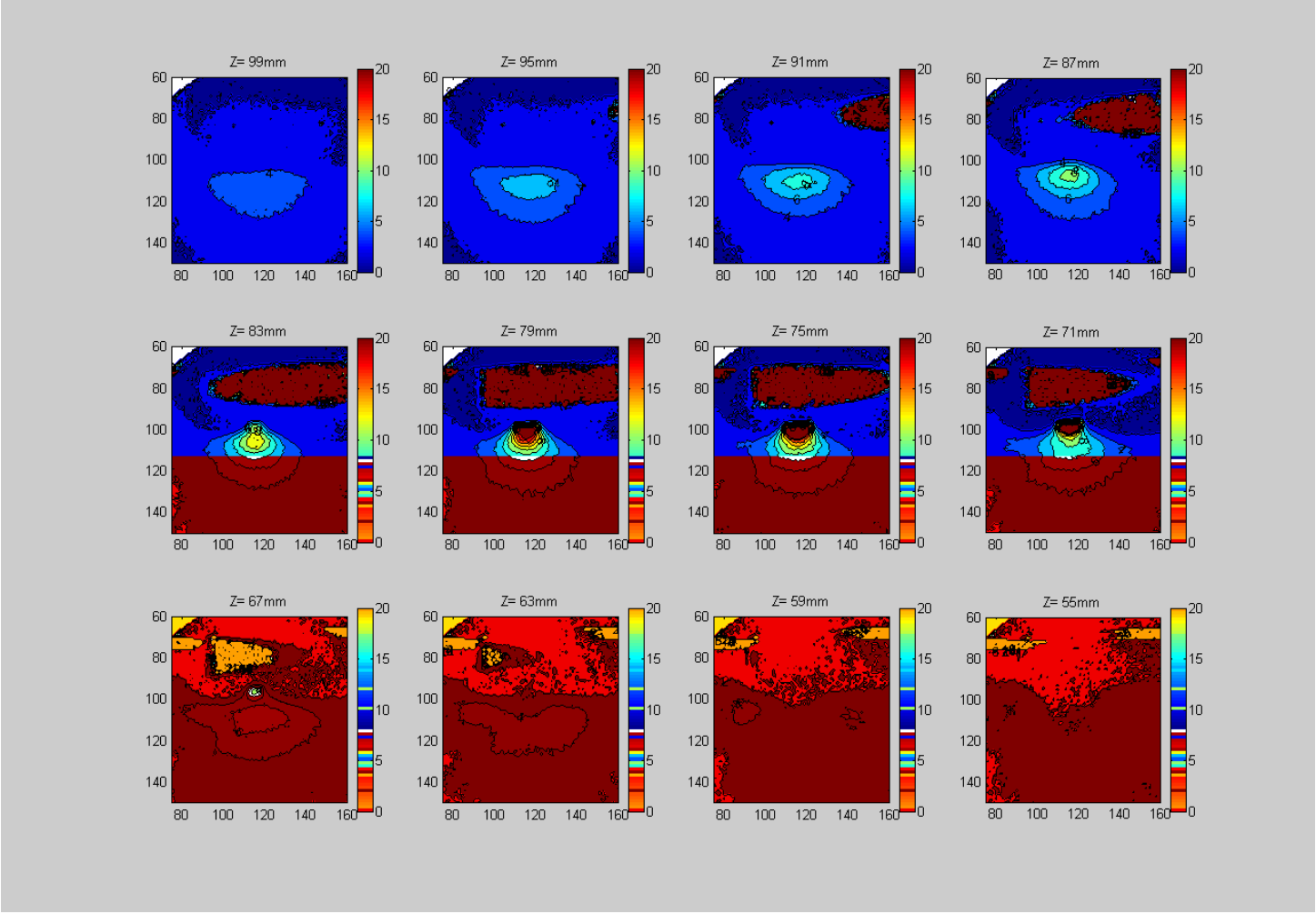

Figure 6.19: The dose mappings in slices of Z=55, 59, 63, 67, 71, 75, 79, 83, 87, 91, 95 and 99 mm in the axial plane of the inhomogeneous phantom, in the paranosal sinuses cavity experiment

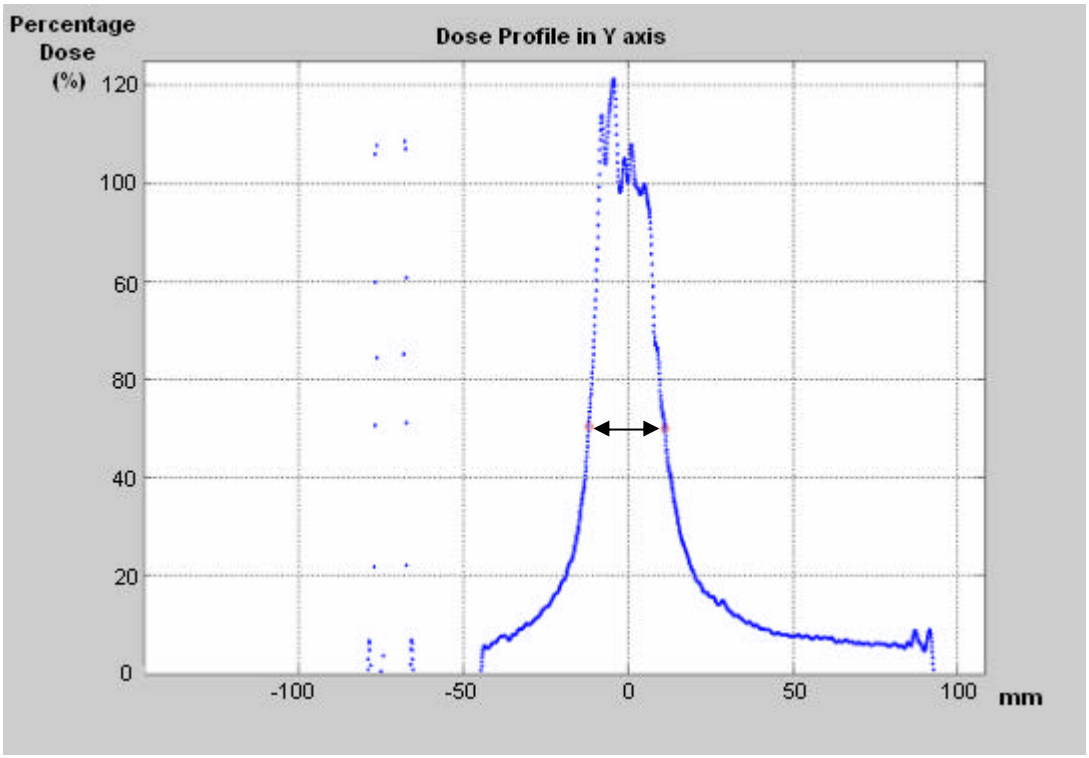

Figure 6.20: The dose profile on the Y axis and the points corresponding to the 50% isodose line in the homogeneous phantom

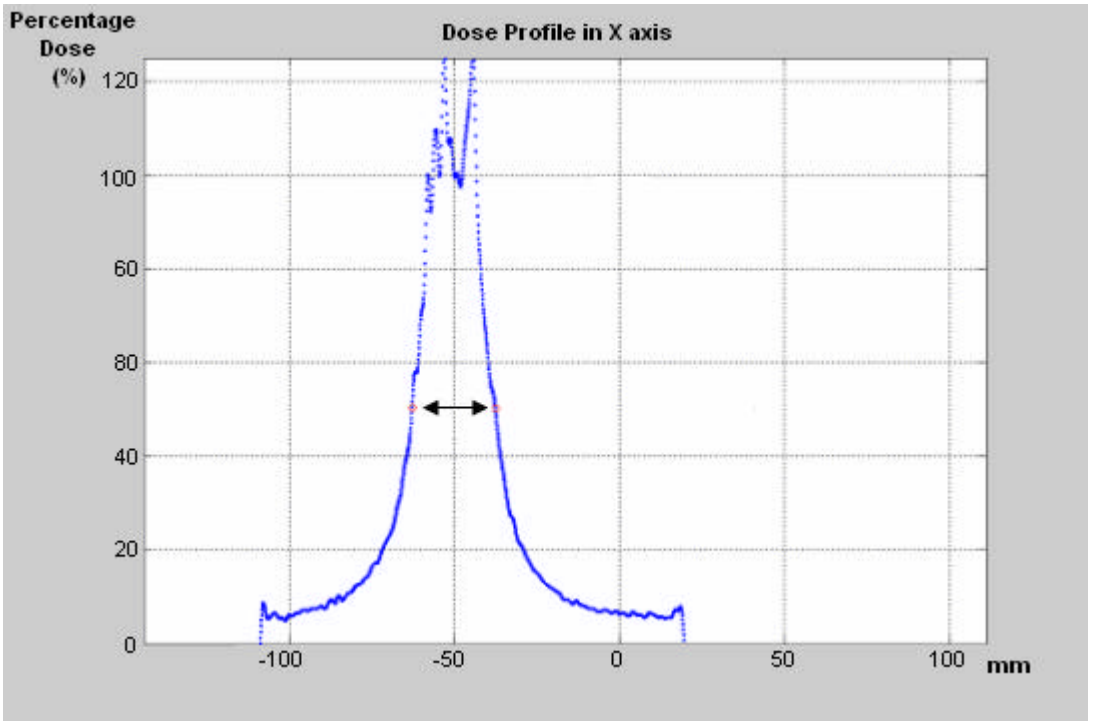

Figure 6.21: The dose profile on the X axis and the points corresponding to the 50% isodose line in the homogeneous phantom

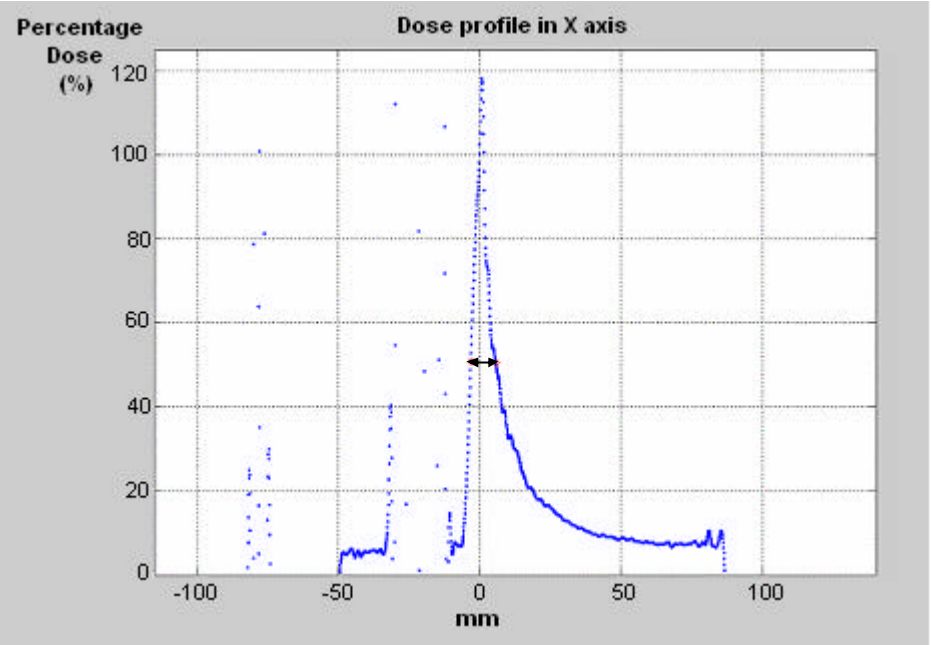

Figure 6.22: The dose profile on the X axis and the points corresponding to the 50% isodose line in the inhomogeneous phantom

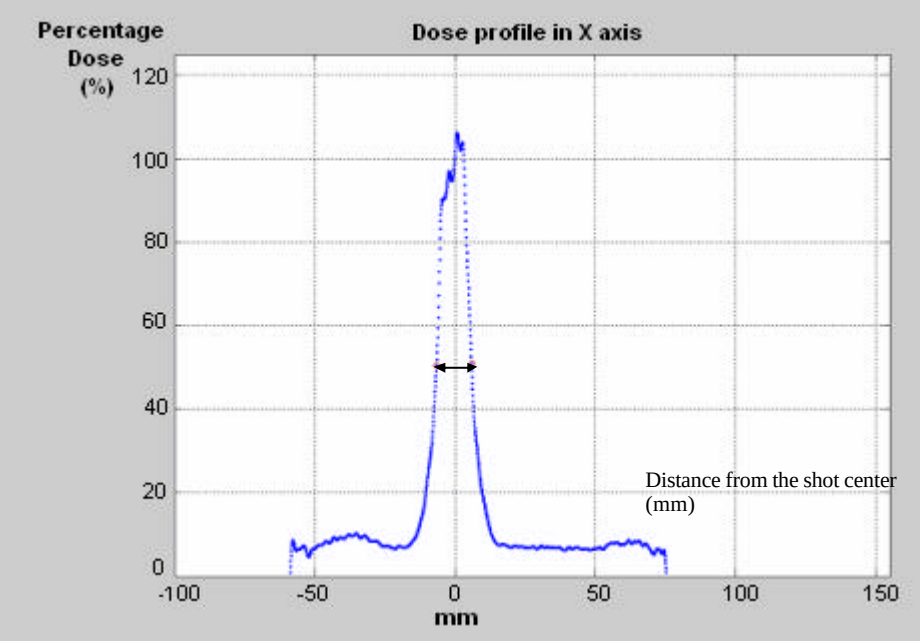

Figure 6.23: The dose profile on the Y axis and the points corresponding to the 50% isodose line in the inhomogeneous phantom

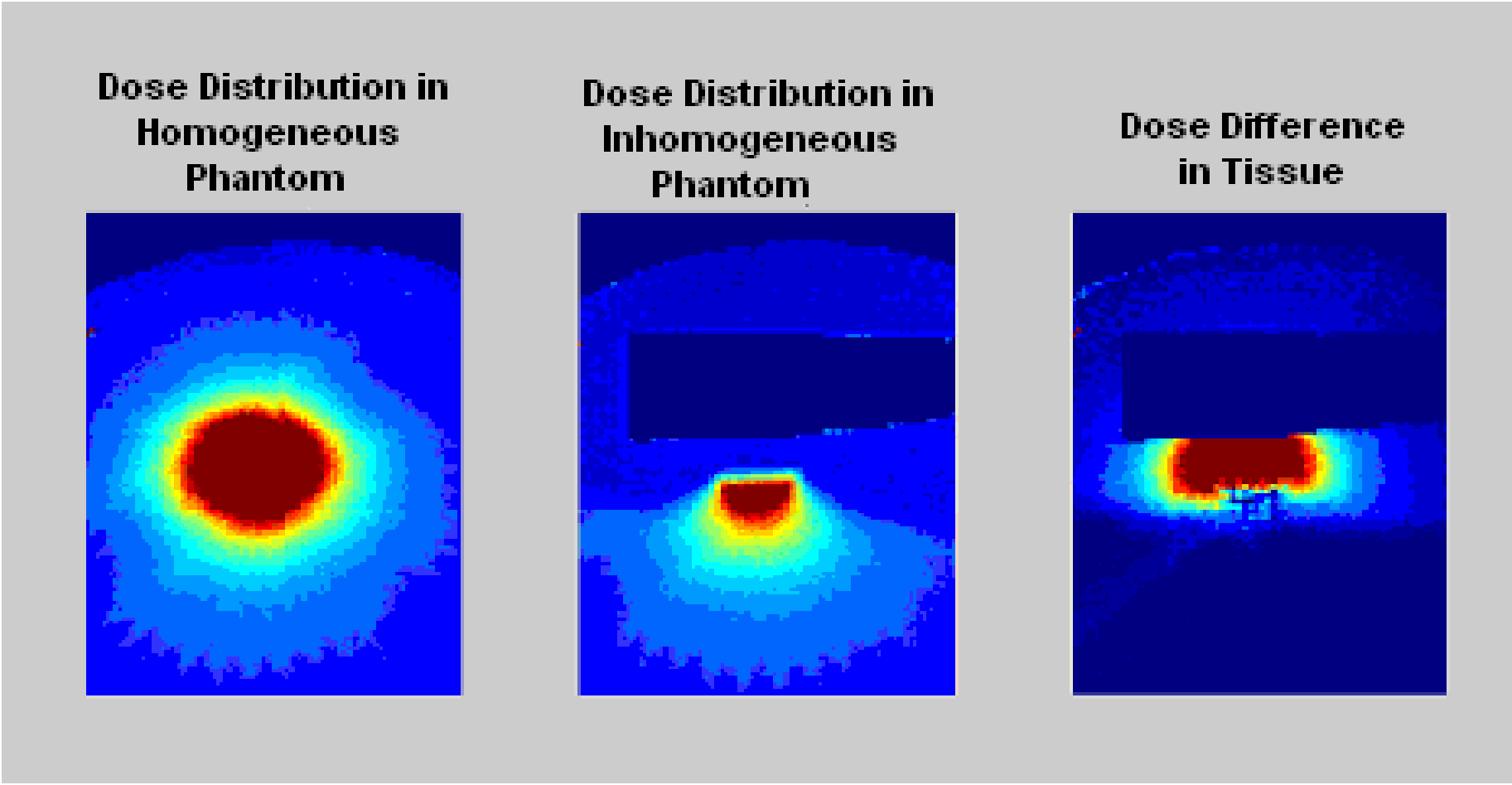

Figure 6.24: Gel dosimetry dose mappings in the axial plane Z=75 mm in the homogeneous phantom (left), the inhomogeneous phantom(middle) and the dose difference between the homogeneous and the inhomogeneous phantoms (right).

Table 6.7: GammaPlan predicted results: Isodose curve diameters in the homogeneous and inhomogeneous phantoms, in the paranosal sinuses cavity simulation.

		Slice (mm)	Leksell Frame	70% Isodose (mm)	50% Isodose (mm)	30% Isodose (mm)
GammaPlan Predicted	Inhomogeneous Phantom	Z=71	X	19,2	23,2	32,4
			Y	18,9	22,9	29,9
		Z=75	X	19,9	24,1	31,8
			Y	19,8	23,6	30,2
		Z=79	X	17,2	20,7	28,3
			Y	16,9	20,2	27,8
	Homogeneous Phantom	Z=71	X	19,1	24,1	33
			Y	18,8	23,6	30,8
		Z=75	X	20	24,5	32,2
			Y	19,9	23,9	31,6
		Z=79	X	17,6	22,7	29,4
			Y	17,6	22,1	29,2

Table 6.8: Gel dosimetry measurements: Isodose curve diameters in the homogeneous and inhomogeneous phantoms, in the paranosal sinuses cavity experiment calculated.

		Slice (mm)	Leksell Frame	70% Isodose (mm)	50% Isodose (mm)	30% Isodose (mm)
Gel Dosimetry Measured	Inhomogeneous Phantom	Z=71	X	10,1	14,2	21,3
			Y	7,7	12,8	21,3
		Z=75	X	12,2	14,6	19,3
			Y	6,3	10,3	18,8
		Z=79	X	8,8	11,3	15,3
			Y	4	6,7	14,2
	Homogeneous Phantom	Z=71	X	19,3	24,4	34,5
			Y	19	24,3	31,7
		Z=75	X	19,6	25,1	32,4
			Y	20,2	25,3	32,9
		Z=79	X	18,2	23,5	31,6
			Y	17,9	22,6	31,3

7. CONCLUSION AND DISCUSSION

Normoxic gel preparation is quite easy which takes nearly 3 hours in the laboratory. The calibration of the gel batches at the predefined doses; followed by scanning in an MR unit with a spin echo sequence, enable us to determine the true T_2 values of the batches. For the MAGIC gel, we observe linearity between the delivered dose and the true T_2 value of the voxel in the gel.

The accuracy of the gel dosimeter depend on that the gel be solid and static in the container and the radiochemical products should not diffuse until the phantom is evaluated in the MR unit. The gel can melt around 30 ^{0}C. Therefore the gel phantoms should be kept in the refrigerator before irradiation.

MAGIC gel dosimetry is a more effective tool as compared to the Fricke gels and other polymer gels, which require avoidance of oxygen. The MAGIC gel can easily be used to calculate the cumulative dose measurement in various radiation therapy modalities.

If one does not consider the air tissue inhomogeneities near the treatment volume such as the air cavities of the sinuses and the auditory canal, the treatment planning in Gamma Knife can lead to serious dose planning inaccuracies. Solberg et all have calculated over 50% of local differences in dose near the air cavity inhomogeneities [59, 60]. Klein et al have reported an underdosing up to 30% in megavoltage beams near the air cavity homogeneities [60,61].

Small photon beams have different characteristics that are not present in large fields of photons such as the rapid decrease of ionization, due to the steep dose gradients and the decrease of the depth maximum, with the decreasing in the field size. These can additionally limit the ion chamber use in the small beam dosimetry. The results indicate that, important amount of perturbation occurs in dose distribution effected by the tissue inhomogeneities. Most treatment planning algorithms cannot predict how the small beams behave when they are perturbed by the air cavities. The reason for this is that, the small beams from the Cobalt 60 sources lose the electronic equilibrium in the presence of air tissue inhomogeneity. In large radiation fields such as those used in the conventional

radiotherapy, this effect is not encountered. Lateral electronic equilibrium at the central axis of the beam is principally performed when the radiation field diameter is at least twice the size of the depth maximum of the beam. In the case of the lateral electronic equilibrium, the central axis of the beam has a spectrum of energy form zero to the maximum photon energy. The electrons with a broad range of energy coming from the sides enter the central axis of the beam. In narrow beams, lateral electronic equilibrium is generally not established. The lower energy photons are usually missing in the energy spectrum. Consequently, for small beams the ratio of the ionization chamber output to the absorbed dose can be larger than the ratio of the corresponding for the broader beams [62,60,59].

The photons are much less attenuated in the air filled cavities compared to the tissue. This increases the dose in the regions behind the air cavities [63].

The 30%, 50% and 70% isodoses change the dose pattern when an air cavity is present adjacently. The air cavity reduces the diameters of the isodoses in the radial axis to the cavity interface. The region in front of the air cavity is underdosed compared to the GammaPlan calculated level of dose. In accordance to the gel phantom in the paranosal cavity simulation, 30%, 50% and 70 % isodoses are at distances of 10, 12 and 15,8 mm away from the shot center, while with the cork representing the air cavity, the same isodoses are at a distance of 2,5, 3,6 and 4,8 mm away from the shot center. This demonstrates the vertical shrinking of the isodose levels. In the auditory canal cavity experiment, the diameter of the 50% isodose curves differ by 35% in the X axis and 1% in the Y axis for Z=105 mm axial plane; and by 39% in the X axis and 5% in the Z axis for Y=105 mm coronal plane in the inhomogeneous phantom as compared to the homogeneous phantom. In the paranosal sinuses cavity experiment, the diameter of the 50% isodose curves differ by 42% in the X axis and %47 in the Y axis for Z=71mm axial plane; 42% in the X axis and %60 in the Y axis for Z=75 mm axial plane; 52% in the X axis and %70 in the Y axis for Z=79 mm axial plane respectively in the inhomogeneous phantom when compared to the homogeneous phantom. The dose decrease near the air-tissue interface causes the GammaPlan's predicted dosage to be higher than that actually delivered. The resulting underdosing effect can be critical for the control of the lesions near tissue inhomogeneities.

The treatment planning aims to cover the tumor or lesion with the 50% isodose line. However, ignoring the tissue inhomogeneities can mislead the exact localization of dose levels. Clinically, this can result in underdosing of the tumor and overdosing of the normal tissue in the unwanted region even if the region is not adjacent to the air cavities [12,68]. These results suggest that the algorithms considering the tissue differences in the head will calculate the delivered dose more precisely. The inhomogeneities in the body will play a more pronounced role in the treatment planning systems, while the treatment techniques for treating the extracranial targets stereotactially develop.

In the simulations, the lack of ability of the GammaPlan to properly account for the impacts of the tissue differences is clearly demonstrated. Since the accuracy in the calculation of dose distribution mapping is at most importance, the inaccuracies that are observed may lead to inability to control lesion or, overdose some critical or undesired tissue in the brain.

Gel dosimetry has the strength of mapping the dose distribution in any slice with arbitrary orientation. The gel can clarify any crossed dose distribution region. The software developed in the thesis can also be used to evaluate gel dosimetry phantoms and for the Quality Assurance processes in other treatment modalities such as Brachytherapy, Intensity Modulated Radiation Therapy, Cyber Knife, and Conventional Radiotherapy. The user interface of the evaluation software can be developed in gel dosimetry. Particularly, gel dosimetry can be deployed as an assessment tool for the treatment planning system of the Gamma Knife. Deployed as a test tool for the complex dose distributions especially, it can clearly demonstrate dose distribution for volumes nearby air cavities.

In the Cyber Knife, which enables conformal radiation treatments, isodose curves may be measured and evaluated by the gel dosimetry. The problem of dose perturbation near the air cavities inhomogeneities related to the electronic disequilibrium will be encountered in the Cyber Knife treatment. The dose distribution especially in volumes near the lungs can be evaluated and compared with the dose distribution predicted by the

treatment planning system of the Cyber Knife. This can be a future study that will be useful in the patient set up procedure.

By the use of gel dosimetry, dose can be estimated in three dimensional space. The dose delivered to any point in a arbitrary shaped gel phantom can be measured with the gel dosimetry.

The dose distribution mappings can be displayed in the axial, coronal, sagittal as well as any arbitrary selected plane. This can be useful in the cases where the amount of dose delivered related to the critical organ protection and tumor control is utmost importance and where the air cavity structures can effect the dose distribution.

Gel dosimetry has the superiority over other dosimetry systems in that it can map the dose distributions, which are the result of multiple radiation sources of radiation. The total polymerization and the change in the true T_2 values have the ability to exhibit the cumulative effect of the total delivered dose from any number of sources.

As long as the Normoxic polymer gel stays solid, the absorbed dose effects remain stable and the gel can be scanned as many times as needed.

REFERENCES

1. Moskvin Vadim, R. Timmerman, C. D. Rosiers, M. Randall, P.D. Rosiers, P. Dittmer and L. Papiez, "Monte Carlo simulation of the Leksell GammaKnife: Effects of heterogeneous versus homogeneous media for stereotactic radiosurgery", Phys. Med. Biol., Vol. 49, pp. 4879–4895, 2004.

2. Wu A, G. Lindner, A. Maitz, A. M. Kalend, L. D. Lunsfond, J. C. Flickinger and W. D. Bloomer, "Physics of Gamma Knife approach on convergent beams in stereotaxic radiosurgery ", Int. J. Radiat. Oncol., Vol. 18 pp. 941–9499, 1990.

3. Wu A, " Physics and dosimetry of the Gamma Knife", Neurosurg. Clin. N. Am., pp. 335–350, 1992.

4. Deene Y, D., C Hurley, Avenning, K. Vergote, M. Mather, B J Healy and C Baldock, "A basic study of some normoxic polymer gel dosimeters", Phys. Med.Biol., Vol. 47, pp. 3441–3463, 2002.

5. Fong P. M., D. C. Keil, M. D. Does and J. C. Gore, "Polymer gels for magnetic resonance imaging of radiation dose distributions at normal room atmosphere", Phys. Med. Biol. 46 3105-3113, 2001

6. Shin M, H. Kurita, T. Sasaki, S. Kawamoto, M. Tago, N. Kawahara, A. Morita, K. Ueki and T. Kirino, "Analysis of treatment outcome after stereotactic radiosurgery for cavernous sinus meningiomas", J. Neurosurg., No: 95, pp. 435–439, 2001.

7. Solberg T. D., F. E. Holly, A. A. F. Desalles, R. E. Wallace and J. B. Smathers "Implications of tissue heterogeneity for radiosurgery in head and neck tumors" Int. J. Radiat. Oncol. 32 235–9, 1995.

8. GENERAL INTRODUCTION INTO THE THREE-DIMENSIONAL GEL DOSIMETRY, http://3dgeldos.fjfi.cvut.cz/generalintro/

9. "Ramani R, M.G. Ketko, P. F. Obrien and M. L. Schwartz, “A QA phantom for dynamic stereotaxic radiosurgery—quantitative measurements”, Med. Phys. Vol. 22, 1343–1346, 1995."

10. Yu C and D. Shepard,"Treatment planning for stereotactic radiosurgery with photon beams" Technol. Cancer. Res.T. 2 93–104. 2003.

11. Technical Description and Specification of Stereotactic Radiosurgery, Elekta Instruments Leksell Gamma Unit Type B, 1992.

12. Duftschmid K. E., P. Kindl, B. Obenaus, C. Strachotinsky and N. Winker “Precision dosimetry in narrow collimated radiation beams of the Leksell Gamma Knife”, Radiat. Prot. Dosim., Vol. 66, pp. 295–298, 1996.

13. Phillips M H, K. J. Stelzer, T. W. Griffin, M. R. Mayberg and H. R. Winn, “Stereotactic radiosurgery: a review and comparisons of methods”, J. Clin. Oncol., Vol. 12,pp. 1085–1099, 1994.

14. Surendra N., A. Rustgi, K. Rustgi, B. Steve, J. Komanduri and M. Ayyangar, “Dose perturbation caused by high-density inhomogeneities in small beams in stereotactic radiosurgery” Phys. Med. Biol, Vol. 43, 3509-3518,1998

15. Heydarian M., P. W. Hobany and A. H. Beddoe, “A comparison of dosimetry techniques in stereotactic radiosurgery”, Phys. Med. Biol., Vol. 41, pp. 93–110, 1996.

16. http://neurosurgery.ucla.edu/Programs/BrainTumor/BrainTumor_Intro.html

17. http://www.irsa.org/publications/IRSAV4_2.pdf.

18. Elekta Public Bulletin- 02/17/1998 “New 4 mm helmet output factor Leksell Gamma Knife” Elekta Instruments, 1998.

19. http://www.cduma.com/GammaKnifeOverview.html

20. http://www.neurosurgery.pitt.edu/imageguided/gammaknife/technical.html

21. http://www.cksociety.org/PatientInfo/radiosurgery_stereotactic_technology_comparisons.asp

22. http://www.irsa.org/radiosurgery.html

23. Judith Gault; Sarin, Hemant.; Awadallah, Nabil A.; Shenkar, Robert.; Awad, Issam A., , "Pathobiology of Human Cerebrovascular Malformations: Basic Mechanisms and Clinical Relevance" Neurosurgery. 55(1): 1-17, July 2004.

24. http://www.irsa.org/publications/IRSAV4_2.pdf.

25. http://www.neurosurgerytoday.org/what/patient_e/stereotactic.asp

26. W. M. Saunders, Winston KR, Siddon RL "Radiosurgery for arteriovenous malformations of the brain using a standard linear accelerator. Rationale and technique", Int J Radiat Biol Phys 15:441-7, 1988.

27. L. Leksell, "The stereotaxic method and radiosurgery of the brain", Acta Chir Scand 102:316-19, 1951.

28. http://www.bcma.org/public/bc_medical_journal/BCMJ/2001/december_2001/Radiosurgery.asp

29. http://www.healthsystem.virginia.edu/internet/neurosurgery/gammaknifeinfo.cfm.

30. http://www.gammaknife.co.uk/internal/Overview/histgamma.pdf

31. Arndt J. and S. Goetsch, "Gamma Knife dosimetry and treatment planning" Med. Phys. Vol.26, pp. 1059-1061, 1999.

32. http://www.medphys.ca/Committees/CAPCA/SRS051024.pdf

33. http://www.braintumorfoundation.org/radiosurgery.asp

34. http://radonc.usc.edu/USCRadOnc/RS/References/ANO97/ANO97.html

35. Louis Lemieuxtt and Roger Jagoet "Effect of fiducial marker localization on stereotactic target coordinate calculation in CT slices and radiographs" Phys. Med. Biol. 39 pp. 1915-1928. 1994.

36. Anna Somigliana, Giovanni Mauro Cattaneo, Claudio Fiorino, Silvana Borelli, Antonella del Vecchio, Giancarlo Zonca, Emanuele Pignoli, Gianfranco Loi, Riccardo Calandrino and Renato Marchesini, "Dosimetry of Gamma Knife and linac-based radiosurgery using radiochromic and diode detectors", *Phys. Med. Biol.* **44** 887-897, 1999.

37. Q. Jackie Wu, Vira Chankong and Suradet Jitprapaikulsarn, Barry W. Wessels and Douglas B. Einstein, Boonyanit Mathayomchan, Boonyanit Mathayomchan, Timothy J. Kinsella, "Real-time inverse planning for Gamma Knife radiosurgery", Medical Physics -- November 2003 -- Volume 30, Issue 11, pp. 2988-2995 .

38. http://www.cs.wisc.edu/~ferris/papers/rad-mip.pdf

39. Joel Y C Cheung, K N Yu, Robert T K Ho and C P Yu, "Monte Carlo calculated output factors of a Leksell Gamma Knife unit", Phys. Med. Biol., 44 pp:247-249, 1999.

40. Helen Gustavsson, Sven A, J Bäck, Joakim Medin, Erik Grusell and Lars E Olsson, "Linear energy transfer dependence of a normoxic polymer gel dosimeter investigated using proton beam absorbed dose measurements" *Phys. Med. Biol.* **49** 3847-3855, 2004.

41. http://users.ugent.be/~esvdbuss/RG/GELDOS_info.htm

42. Chu W. C. “Radiation Dosimetry Using Fricke-infused Gels and Magnetic Resonance Imaging, MRI-Fricke-infused Gel Dosimetry”, Proc. Natl. Sci. Counc. , Vol. 25, pp. 1-11, 2001.

43. Scheib S. G., Y. Schenkel and S. Gianolini, “Absolute dose verifications in small photon fields using BANG TM gel”, Journal of Physics: Conference Series 3, pp.228–231, Third International Conference on Radiotherapy Gel Dosimetry, 2004.

44. Deene Y. De., “Essential characteristics of polymer gel dosimeters”, Journal of Physics: Conference Series 3, Third International Conference on Radiotherapy Gel Dosimetry, pp.34-57, 2004.

45. L J Schreiner, “ Review of Fricke gel dosimeters”, Third International Conference on Radiotherapy Gel Dosimetry, Journal of Physics: Conference Series 3, pp. 9–21. 2004.

46. Schacht E. H., “Polymer chemistry and hydrogel systems”, Journal of Physics: Conference Series 3, Third International Conference on Radiotherapy Gel Dosimetry, pp.22–28, 2004.

47. M Mcjury, M. Oldham, P. Cosgrove, S. Murphy, S. Doran, M. O. Leach and S Webb, “Radiation dosimetry using polymer gels: methods and applications”, The British Journal of Radiology, Vol. 73, pp. 919929, 2000.

48. Novotny J. Jr., V. Spevacek, J. Hrbacek, L. Judas, J.Novotny, P. Dvorak, D.Tlachacova, M. Schmitt, J.Tintera, J. Vymazal, T. Cechak, J. Michalek, M. Pradny and R. Liscak “Measurement Of Relative Dose Distributions In Stereotactic Radiosurgery by The Polymer Gel Dosimeter” Radiosurgery Society Congress Kyoto, Japan, 2003.

49. Scheib S. G. and W. Vogelsanger, “MAGIC - Normoxic Polymer Gel Dosimetry in Radiosurgery.” Kondziolka D (ed): Radiosurgery. Basel, Karger, Vol 5, pp. 213-224, 2004.

50. http://www.cksociety.org/PatientInfo/MedicalConditions/arteriovenous_malformation.asp#advantages_avm.

51. Maryanski M.J., R.J.Schulz, G.S. Ibott, J.C. Gatenby, J. Xie, D. Horton and J.C. Gore "Magnetic resonance imaging of radiation dose distributions using a polymer-gel dosimeter" Phys. Med. Biol. Vol.39, pp. 1437-1455,1994.

52. http://etd02.lnx390.lsu.edu/ docs/available/etd-0305103-43757/unrestricted/ literaturereview.pdf

53. Deene Y, D., C Hurley, Avenning, K. Vergote, M. Mather, B J Healy and C Baldock, "A basic study of some normoxic polymer gel dosimeters", Phys. Med.Biol., Vol. 47, pp. 3441–3463, 2002.

54. Fong P. M., D. C. Keil, M. D. Does and J. C. Gore, "Polymer gels for magnetic resonance imaging of radiation dose distributions at normal room atmosphere", Phys. Med. Biol. 46 3105-3113, 2001.

55. Deene Y. D., "A history of polymer gel"Medical Physics, 12, pp: 77-88, 2002.

56. Baldock Clive, "Historical overview of gel dosimetry, Journal of Physics": Conference Series 3, Third International Conference on Radiotherapy Gel Dosimetry, 1-3, 2004.

57. http://www.science.doe.gov/bes/chm/Publications/WaterWorkshopReport_final.pdf

58. Amin M. N., D. E. Bonnett and M. A. Horsfield, "Normoxic polymer gels: are they magic?", Journal of Physics: Conference Series 3, Third International Conference on Radiotherapy Gel Dosimetry, pp.192-195, 2004.

59. Solberg T. D., "Application of radiation Transport methods to small field dosimetry in heterogeneous Media", PhD. Thesis, 1996.

60. Klein E., E. Chin, R.K. Rice and B.J. Minjnheer “The influence of air cavities on interface doses for photon beams” Int. J. Radiation Oncology Biol. Phys. 27, pp. 419-427,1993.

61. Bussche E. V., Y. D. Deene, K. Vergote and C. D. Wagter, “Alternative gelling agents for normoxic gels: a stability study”, Journal of Physics: Conference Series 3, Third International Conference on Radiotherapy Gel Dosimetry, 168-171, 2004.

62. Verhaegen F “Interface perturbation effects in high-energy electron beams” Phys. Med. Biol. Vol. 48 pp. 687–705, 2003.

63. Duftschmid K. E., P. Kindl, B. Obenaus, C. Strachotinsky and N. Winker “Precision dosimetry in narrow collimated radiation beams of the Leksell Gamma Knife”, Radiat. Prot. Dosim., Vol. 66, pp. 295–298, 1996.